Cement and Concrete Research 40 (2010) 1360–1374

Contents lists available at ScienceDirect

Cement and Concrete Research

journal homepage: http://ees.elsevier.com/CEMCON/default.asp

Chemical model for cement-based materials: Thermodynamic data assessment for phases other than C–S–H

Ph. Blanc [a,*], X. Bourbon [b], A. Lassin [a], E.C. Gaucher [a]

[a] BRGM, 3 Avenue Claude Guillemin, 45060 Orléans Cedex 2, France
[b] ANDRA — Scientific Division, 1-7 Rue Jean Monnet, Parc de la Croix Blanche, 92298 Chatenay Malabry Cedex, France

ARTICLE INFO

Article history:
Received 23 February 2009
Accepted 19 April 2010

Keywords:
Sulfoaluminate (D)
Hydrogarnet (D)
Chloride (D)
Thermodynamic calculations (B)
Temperature (A)

ABSTRACT

In the context of waste confinement, concrete may be used both as a confinement and as a building material. Concerning radwaste, the heat released during radioactive decay will modify the equilibrium constants of the minerals forming the concrete. The present work aims to elucidate the temperature dependency of the thermodynamic functions related to minerals from the concrete or associated with some of its degradation products. A large set of experimental data has been collected, for the chemical systems SO_3–Al_2O_3–CaO–CO_2–Cl–H_2O and SiO_2–Al_2O_3–CaO–H_2O, including iron and magnesium bearing phases. Most of the data collected concern experiments in aqueous media but results from calorimetric studies were also included, when available. Based on selected thermodynamic properties for each phase, predominance diagrams were drawn for the chemical elements listed above. Phase relations reported into predominance diagram appear rather consistent with most of the literature results. The case of katoite has been especially discussed, because it shows inconsistencies with respect to a hydrogarnet–grossular solid solution and with respect to phase relations reported into already published works. Finally, we underline the chemical compatibility of Portland cement pastes with carbonate aggregates, compared to silicates, for long-term storage applications.

1. Introduction

The application domain of thermodynamic equilibria in cementitious media is large, especially in the context of long-term disposal. A particularly interesting case concerns the building of underground facilities for storing high to medium-level, long lived radioactive waste, where concrete is used in particular as a supporting material for the access galleries to the storage cells.

The present wok comes along a first study concerning the phases which belong to the system CaO–SiO_2–H_2O (C–S–H) [1]. The authors had investigated phase relations and the thermodynamic properties of nanocrystalline and crystalline C–S–H, taking into account the influence of temperature. In order to complete the mineral set, the present study aims to define the solubility constants of the other mineral phases that constitute the concrete or which are produced during the degradation processes. Different works had been published to date concerning either the solubility of these phases (case of ettringite [2,3]) or phase relations for more complex mineralogical assemblages [4,5]. Recently, an important work by Matschei et al. [6] had provided new solubility data for a large set of minerals belonging to the cementitious chemical system.

The present study aims to collect, to gather and to synthesize most of the experimental data available for cementitious media, into a consistent thermodynamic database. Our selection is consistent with the more general thermodynamic databases Thermochimie6 [7] and Thermoddem [8]. It is also especially dedicated to the temperature dependence of the equilibrium constants. Indeed, the radioactive decay reactions occurring within containers produce heat which implies an increase of temperature in the disposal environment. A geochemical model describing the long-term behaviour of containment materials must then take into account temperatures ranging from 10 to around 100 °C. This implies to focus especially the selection of thermodynamic constants not only on the equilibrium constants but also on the enthalpy of formation and the heat capacity of the minerals.

In addition, this work is focussed on small chemical systems, related to cement chemistry. The present study proposes two main parts. Thermodynamic properties are first selected or extracted for each single phase. Then, phase relations are investigating for different chemical systems through predominance diagrams, in a way to assess the consistency of our selection.

2. Context and theoretical tools

2.1. Framework for the selection of thermodynamic data

The present work is based on a previous selection for aqueous complexes [7] for the Thermochimie6 and Thermoddem databases. The Thermochimie6 database has been developed to meet the needs of ANDRA in terms of geochemical modelling while the Thermoddem

* Corresponding author. Tel.: +33 2 38 64 39 92; fax: +33 2 38 64 30 62.
E-mail address: p.blanc@brgm.fr (P. Blanc).

0008-8846/$ – see front matter © 2010 Elsevier Ltd. All rights reserved.
doi:10.1016/j.cemconres.2010.04.003

database has been designed within the framework of waste (municipal of industrial) storage and more general environmental studies.

The two databases rely on CODATA recommendations [9] for the primary master species and the reference states of the elements. Recent advances have been made, particularly for aluminium and silicon [7,10,11], which have led us to modify the properties of formation of the aqueous species Al^{+++} and H_4SiO_4. In addition, the two databases have adopted the NEA recommendations [12–14], in particular as regarding the dependence of ionic strength and temperature on the thermodynamic properties.

For the remainder of this work, the master species for expressing equilibria in aqueous solutions are Al^{+++}, Ca^{++}, H_4SiO_4, Ca^{++}, Mg^{++}, Fe^{+++}, CO_3^{--}, Cl^-, SO_4^{--}, H_2O and H^+. The convention used to define the standard state of the compounds in the present work, and also in the Thermoddem database, is that proposed by Helgeson et al. [15].

In this work, mineral/solution equilibria are calculated using PHREEQC [16] and GWB [17] software, using the extended Debye–Hückel activity coefficient model.

Table 1 gives the list of complexes retained in this study. The selection is discussed in Blanc et al. [7].

2.2. Equations and notations used

The thermodynamic relations used in this work are identical to those employed by Blanc et al. [1] and we will therefore provide only a brief outline of these relations.

One considers the equilibrium constant of the dissolution/precipitation reaction $AB \leftrightarrows A^+ + B^-$, at the pressure and temperature of reference P_r and T_r. It is related to the standard free enthalpy of reaction $\Delta_r G^\circ_{AB,P_r,Tr}$ by the following relation:

$$\Delta_r G^\circ_{AB,Pr,Tr} = -R\cdot Tr\cdot \log K_{AB,Pr,Tr}\cdot \ln(10) \quad (1)$$

where $R = 8.314472\ J\ mol^{-1}\ K^{-1}$ is the gas constant.

The standard free enthalpy of reaction is obtained by subtracting the standard free enthalpy of formation of the reaction components. Following the Helgeson et al. [15] convention, the AB Gibbs free energy $\Delta_f G^\circ_{AB,P,T}$ depends on temperature, according to the relation:

$$\begin{aligned}\Delta_f G^\circ_{AB,P,T} &= \Delta_f H^\circ_{AB,P,T} - T\cdot S^\circ_{AB,P,T} \\ &= \Delta_f H^\circ_{AB,Pr,Tr} - T\cdot S^\circ_{AB,Pr,Tr} + \int_{Tr}^{T} Cp_{AB}\,dT - \int_{Tr}^{T} \frac{Cp_{AB}}{T}\,dT + \int_{Pr}^{P} V_{AB}\,dP\end{aligned} \quad (2)$$

where:

- $\Delta_f H^\circ_{AB,P,T}$ standard enthalpy of formation of the phase AB, at the temperature T and the pressure P
- $S^\circ_{AB,P,T}$ third-law standard entropy of the phase AB, at the temperature T and the pressure P
- Cp_{AB} Heat capacity of the phase AB; $Cp_{AB} = a_{AB} + b_{AB}\cdot T + c_{AB}/T^2$
- V^0_{AB} Molar volume of the phase AB, independent of temperature in our case.

When the equilibrium is reached for the reaction $AB \rightarrow A^+ + B$, the ionic activity product IAP_{AB} equals the equilibrium constant, which leads to:

$$K_{AB}(T) = IAP_{AB} = \left(A^+\right)\cdot\left(B^-\right) = \gamma_{A^+}\cdot\left[A^+\right]\cdot\gamma_{B^-}\cdot[B^-] \quad (3)$$

where (A^+), $[A^+]$ and γ_{A+} correspond respectively to the activity, the concentration and the activity coefficient of the cation A^+.

In addition, we have adopted a convention widely used for cementitious materials. We have used the following notations to designate chemical formula of minerals: C = CaO; S = SiO_2; A = Al_2O_3, M = MgO, F = Fe_2O_3 and H = H_2O.

3. Selection of thermodynamic constants

In the selection presented here, we have proceeded for each mineral the following way:

- the equilibrium constant at 25 °C is selected from a single experimental work
- the formation enthalpy and the Cp(T) function are taken from the literature or estimated
- finally the Log$K$(T) function is calculated, based on the select dataset and it is compared to experimental data gathered at different temperatures. Each experimental point is extracted from solution compositions by using PHREEQC with the aqueous complexes reported in Table 1 for sake of consistency.

Including calorimetric measurements or even estimated values for the Cp(T) and the formation enthalpy avoids to rely only on equilibration experiments.

For the equilibration experiments in aqueous media, we have tried to retain only the aqueous solutions displaying an ionic charge imbalance smaller than 5%. Indeed, in some cases, the discrepancy is higher. According to Myeni et al. [2], this problem can arise either from impurities in aqueous solution, namely the carbonation of the system. This corresponds to a particular case of "pollution" of the theoretical chemical system by foreign elements. This situation is not surprising in cementitious systems in so far as aqueous solutions are systematically alkaline and strongly basic. Charge imbalances in aqueous solution may also result from analytical uncertainties, especially when the concentrations analysed reach the detection limit.

For equilibrium constant selection, we have also considered the duration and the reversibility of the experiments considered, in addition to the electroneutrality of the solutions.

The thermodynamic constants finally selected here are given in Table 2, together with the equilibration reactions considered.

3.1. CaO–Al_2O_3–SO_3–H_2O system

The phases belonging to this system (ettringite, monosulfoaluminate, C4AH13 and C3AH6) have been much studied for different reasons. First, the precipitation of secondary ettringite ($Ca_6Al_2(SO_4)_3(OH)_{12}\cdot 26H_2O$) can be responsible for swelling in concrete, leading to fissuring of the material and a loss in compressive strength. In addition, ettringite and monosulfoaluminate can incorporate other anionic groups, such as chromates for example [38]. This makes it a material particularly suited for the stabilization of waste. Thermodynamic properties of ettringite, monosulfoaluminate and C3AH6 collected in literature are reported in Table 3.

3.1.1. Hydrogarnet, C3AH6

Different studies have already been published, concerning the solubility of hydrogarnet C3AH6 [5,6,39,40]. Solubility constants calculated from the experimental data found in literature are reported in Fig. 1. Most of the authors do not report the pH of the solutions, preventing to test the electroneutrality. On the other hand, Matschei et al. [6] and Glasser et al. [41] have reported pH values showing an electroneutrality discrepancy less than 1% in both studies. Glasser et al. [41] have used longer reaction times (173 days against 84 days for Matschei et al. [6]). From the solution composition provided by Glasser et al. [41], we have extracted a 25 °C equilibrium constant, Log$K$ = 80.38, that moves to 80.32 when pH is corrected for strict electroneutrality. This latter value is slightly lower than Log$K$ = 80.94 obtained by considering Matschei et al. [6] solution compositions. Finally, we retained Log$K$ = 80.32 because of a longer reaction time in Glasser et al. [41] experiments.

The Log$K$(T) function was calculated from the present selection presented in Fig. 1. It is obtained by selecting the value 80.32 for the equilibrium constant at 25 °C and the Cp(T) function determined

Table 1
Thermodynamic database for aqueous complexes and elements.

Phase	Log$K(298)^{(**)}$	$\Delta_f G°_{Pr,Tr}$ kJ mol^{-1}	$\Delta_f H°_{Pr,Tr}$ kJ mol^{-1}	$S°_{Pr,Tr}$ J mol^{-1} K^{-1}	Reference	Cp(298) J mol^{-1} K^{-1}	Cp(T) function calculation
System H_2O							
H_2O	(*)	*−237.14*	−285.83	69.95	[9], [26]	75.35	State equation published by IAPW [26]
O_2,aq	*−85.99*	*16.53*	−12.13	109.00	[19]	234.30	HKF coefficients from [19]
H_2,aq	*−3.08*	*17.56*	−4.20	57.70	[24]	166.94	HKF coefficients from [19]
H^+	(*)	*0.00*	0.00	0.00	Convention, [9]	0.00	By convention, [18]
OH^-	*−14.00*	*−157.22*	−230.02	−10.90	[9]	−137.19	HKF coefficients from [20]
e−	(*)	*0.00*	0.00	65.34	Convention,[9]	14.42	By convention, [9]
Silica complexes							
$H_4SiO_{4,aq}$	(*)	*−1309.23*	−1461.19	180.77	See text	198.86	See text
$AlH_3SiO_4^{+2}$	−2.38	*−1783.28*	*−1922.21*	56.78	[21]	−300.83	HKF coefficients from [21]
$H_2SiO_4^{-2}$	−23.14	*−1177.14*	−1386.72	*−12.58*	[25]	−80.00	[22]
$Ca(H_3SiO_4)^+$	−8.83	*−1811.63*	*−1972.56*	61.62	[23]	212.88	HKF coefficients from [23]
$Mg(H_3SiO_4)^+$	−8.58	*−1715.63*	*−1901.08*	−29.55	[23]	233.59	HKF coefficients from [23]
$H_3(SiO_4)^-$	−9.84	*−1253.06*	*−1431.83*	90.87	[23]	−12.51	HKF coefficients from [23]
NaH_3SiO_4,aq	−8.01	*−1525.46*	*−1693.81*	111.79	[23]	178.32	HKF coefficients from [23]
Other complexes							
Al^{+++}	(*)	−487.64	−538.40	*−337.97*	[27]	−103.22	HKF coefficients from [27]
$Al(OH)_4^-$	*−22.87*	*−1305.64*	−1500.84	110.61	[27]	85.68	HKF coefficients from [27]
$KAl(OH)_4$	*−24.22*	*−1580.45*	−1722.19	289.27	[28]	237.93	HKF coefficients from [28]
$NaAl(OH)_4$	*−23.63*	*−1563.28*	−1731.71	186.34	[27]	291.08	HKF coefficients from [27]
Ca^{+2}	(*)	*−552.81*	−543.00	−56.20	[9]	−31.51	HKF coefficients from [20]
$CaCl^+$	−0.29	*−682.37*	*−702.93*	18.83	[23]	73.10	HKF coefficients from [23]
$CaCO_3$	*−7.11*	*−1099.09*	−1203.40	5.19	[23]	−123.85	HKF coefficients from [23]
$CaOH^+$	−12.78	*−717.00*	−751.62	28.03	[30]	5.86	HKF coefficients from [29]
$CaSO_4$	2.31	*−1310.00*	*−1448.05*	20.92	[31]	−104.60	HKF coefficients from [23]
Cl^-	(*)	*−131.22*	−167.08	56.60	[9]	−122.12	HKF coefficients from [29]
CO_3^{-2}	*−10.33*	*−527.90*	−675.23	−50.00	[9]	−288.29	HKF coefficients from [29]
HCO_3^-	(*)	*−586.85*	−689.93	98.40	[9]	−35.09	HKF coefficients from [29]
Fe^{++}	(*)	*90.53*	−90.00	−101.58	[29]	−33.05	HKF coefficients from [29]
Fe^{+++}	*8.49*	*−162.80*	−49.00	−278.44	[29]	−77.42	HKF coefficients from [29]
$Fe(OH)_4^-$	−21.60	*−841.55*	*−1053.03*	55.00	[29]	−496.00	HKF coefficients from [29]
K^+	(*)	*−282.51*	−252.14	101.20	[9]	25.54	HKF coefficients from [20]
KCl	−0.50	*−410.87*	*−415.04*	162.26	[33]	−34.73	HKF coefficients from [32]
KOH	−14.46	*−437.11*	*−471.53*	117.15	[34]	−85.77	HKF coefficients from [32]
KSO_4^-	0.88	*−1031.54*	*−1158.53*	146.44	[23]	−45.60	HKF coefficients from [23]
Mg^{+2}	(*)	*−455.38*	−467.00	−137.00	[9]	−22.34	HKF coefficients from [20]
$MgCO_3$	2.98	*−1000.29*	*−1133.43*	−100.42	[23]	−114.64	HKF coefficients from [23]
$MgOH^+$	−11.68	*−625.85*	*−690.00*	−79.91	[29]	128.87	HKF coefficients from [29]
Na^+	(*)	*−261.95*	*−240.34*	58.45	[9]	37.91	HKF coefficients from [20]
NaCl	−0.50	*−390.32*	*−405.42*	112.19	[33]	35.57	HKF coefficients from [23]
$NaCO_3^-$	1.27	*−797.10*	*−878.19*	158.12	[35]		
NaOH	−14.75	*−414.90*	*−472.78*	25.10	[27]	−13.39	HKF coefficients from [27]
$NaSO_4^-$	0.94	*−1011.32*	*−1152.49*	85.52	[36]	20.92	HKF coefficients from [36]
SO_4^{-2}	(*)	*−744.00*	*−909.34*	18.50	[9]	−267.05	HKF coefficients from [20]
Elements in their reference state, at 25 °C and 1 bar							
O_2,g	*−83.09*	*0.00*	0.00	205.15	[9]	29.38	Cp(298), [9]
H_2,g	*0.00*	*0.00*	0.00	130.68	[9]	28.84	Cp(298), [9]
Al,cr	*−85.43*	*0.00*	0.00	28.30	[9]	24.20	Cp(298), [9]
Si,cr	*−63.19*	*0.00*	0.00	18.81	[9]	19.79	Cp(298), [9]
Ca,cr	*−96.85*	*0.00*	0.00	41.59	[9]	25.93	Cp(298), [9]
K,cr	*70.99*	*0.00*	0.00	64.68	[9]	29.60	Cp(298), [9]
Na,cr	*67.39*	*0.00*	0.00	51.30	[9]	28.23	Cp(298), [9]
Mg,cr	*122.77*	*0.00*	0.00	32.67	[9]	24.87	Cp(298), [9]
Fe,cr	*58.85*	*0.00*	0.00	27.32	[18]	25.10	Calculated from [18] data
C,cr	*64.16*	*0.00*	0.00	5.74	[9]	8.52	Cp(298), [9]
Cl_2,g	*2.98*	*0.00*	0.00	223.08	[9]	33.95	Cp(298), [9]
S,cr	*93.15*	*0.00*	0.00	32.05	[9]	22.75	Cp(298), [9]

Properties in italics have been recalculated using the values in normal characters; (*) primary master species; (**) for the equilibrium constant are calculated by using the primary master species.

experimentally by Ederova and Satava [50]. For the enthalpy of formation, we have retained the value -5551.50 ± 16.40 kJ/mol, from calorimetric measurements performed by Shoenitz and Navrotsky [51].

3.1.2. Ettringite (AFt-SO_4)

As for the preceding case, a lot of papers had been published about the solubility of ettringite. The experimental studies finally retained in accordance with the selection criteria are listed in Table 4. This table also indicates the values of the equilibrium constants obtained by adjusting the pH value for the sake of electroneutrality. We have selected the 25 °C equilibrium constant calculated by means of Warren and Reardon [53] experimental results, i.e. Log$K = 56.97 \pm 0.50$. In that case, Log$K$ values obtained by adjusting or not pH are identical. Furthermore, equilibrium is reached from both under and supersaturation. In Fig. 2, we have reported the equilibrium constant calculated as a function of temperature by using the value already selected, the Cp(T) function

Table 2
Thermodynamic properties for cementitious phases, selected or estimated in this work.

Name	Reaction	Log*K*(298)	$\Delta_f G^\circ_{Pr,Tr}$ kJ mol^{-1}	$\Delta_f H^\circ_{Pr,Tr}$ kJ mol^{-1}	$S^\circ_{Pr,Tr}$ J mol^{-1}	Cp(298) J mol^{-1} K^{-1}	*a* J mol^{-1}	$b*10^3$ J mol^{-1} K^{-2}	$c*10^{-5}$ J mol^{-1} K	*V* cm^3 mol^{-1}
$CaO–Al_2O_3–SiO_2–H_2O$ system										
Grossular	$Ca_3Al_2Si_3O_{12} + 12H^+ = 2Al^{+++} + 3Ca^{++} + 3H_4SiO_4$	*49.35*	*−6279.46*	−6640.00 [a]	260.10 [a]	326.50 [a]	435.21 [a]	71.18 [a]	−114.30 [a]	125.28 [a]
Katoite	$Ca_3Al_2(SiO_4)(OH)_8 + 12H^+ = 2Al^{+++} + 3Ca^{++} + 8H_2O + H_4SiO_4$	71.16 [c]	*−5433.82*	*−5907.82*	364.00 [E]	415.07 [E]				141.51 [E]
Straetlingite	$Ca_2Al_2SiO_2(OH)_{10}\cdot 2.5H_2O + 10H^+ = 2Al^{+++} + 2Ca^{++} + 10.5H_2O + H_4SiO_4$	49.66 [c]	*−5596.58*	*−6216.78*	545.88 [E]	521.48 [E]				215.63 [b]
$CaO–Al_2O_3–SO_3–CO_2–Cl–H_2O$ system										
Ettringite	$Ca_6Al_2(SO_4)_3(OH)_{12}\cdot 26H_2O + 12H^+ = 2Al^{+++} + 6Ca^{++} + 38H_2O + 3SO_4^{--}$	56.97 [d]	*−15210.23*	−17544.53 [f]	*1883.59*	2174.36[g]	1939.12[g]	789.00[g]		710.32 [i]
Monosulfoaluminate	$Ca_4Al_2(SO_4)(OH)_{12}\cdot 6H_2O + 12H^+ = 2Al^{+++} + 4Ca^{++} + 18H_2O + SO_4^{--}$	73.07 [c]	*−7781.90*	−8763.68 [c]	*786.94*	942.42[g]	594.18[g]	1168.00[g]		311.26 [i]
Hydrogrossular	$Ca_3Al_2(OH)_{12} + 12H^+ = 2Al^{+++} + 3Ca^{++} + 12H_2O$	80.32 [c]	*−5020.87*	−5551.50[h]	*416.61*	459.35[g]	292.09[g]	561.00[g]		149.52 [a]
C4AH13	$Ca_4Al_2(OH)_{14}\cdot 6H_2O + 14H^+ = 2Al^{+++} + 4Ca^{++} + 20H_2O$	103.65 [c]	*−7337.63*	−8318.00[k]	*685.13*	798.90 [E]				269.20 [j]
Monocarboaluminate	$3CaO\cdot Al_2O_3\cdot CaCO_3\cdot 10.68H_2O + 13H^+ = 2Al^{+++} + HCO_3^- + 4Ca^{++} + 16.68H_2O$	80.55 [c]	*−7269.02*	−8175.75 [f]	*601.89*	730.82 [E]				261.96 [j]
Hemicarboaluminate	$6CaO\cdot 2Al_2O_3\cdot CaCO_3\cdot Ca(OH)_2\cdot 21H_2O + 27H^+ = 4Al^{+++} + HCO_3^- + 8Ca^{++} + 37H_2O$	183.66 [c]	*−14685.62*	*−16600.31*	1269.09 [E]	1531.53 [E]				569.02 [j]
Friedel's salt	$2Ca_2Al(OH)_6Cl\cdot 2H_2O + 12H^+ = 2Al^{+++} + 4Ca^{++} + 2Cl^- + 16H_2O$	74.93 [c]	*−6815.44*	−7670.04[k]	*527.70*	692.86 [E]				276.24 [j]
Mg bearing phases										
Hydrotalcite	$Mg_4Al_2(OH)_{14}\cdot 3H_2O + 14H^+ = 2Al^{+++} + 4Mg^{++} + 17H_2O$	73.74 [c]	*−6407.21*	*−7219.64*	512.96 [E]	556.15 [E]				227.36 [j]
Hydrotalcite–CO3	$Mg_4Al_2(OH)_{12}(CO_3)\cdot 2H_2O + 13H^+ = 2Al^{+++} + HCO_3^- + 4Mg^{++} + 14H_2O$	61.19 [n]	*−6295.37*	*−7078.83*	552.07	604.15 [E]				231.46 [j]
Brucite	$Mg(OH)_2 + 2H^+ = Mg^{++} + 2H_2O$	17.10[m]	*−832.05*	−924.50[m]	*58.42*	77.27[m]	102.20[m]	15.11[m]	−26.17[m]	24.63 [a]
Fe bearing phases										
C4FH13	$Ca_4Fe_2(OH)_{14}\cdot 6H_2O + 14H^+ = 2Fe^{+++} + 4Ca^{++} + 20H_2O$	*95.12*	*−6443.63*	−7417.40 [o]	705.35 [E]	787.08 [E]				274.40 [j]
C3FH6	$Ca_3Fe_2(OH)_{12} + 12H^+ = 2Al^{+++} + 3Ca^{++} + 12H_2O$	*72.37*	*−4123.57*	−4647.59 [o]	436.84 [E]	484.15 [E]				154.50 [j]
Ettringite-Fe	$Ca_6Fe_2(SO_4)_3(OH)_{12}\cdot 26H_2O + 12H^+ = 2Fe^{+++} + 6Ca^{++} + 38H_2O + 3SO_4^{--}$	54.55 [c]	*−14281.38*	*−16601.22*	1930.11 [E]	2214.54 [E]				711.80 [j]
Monosulfate-Fe	$Ca_4Fe_2(SO_4)(OH)_{12}\cdot 6H_2O + 12H^+ = 2Fe^{+++} + 4Ca^{++} + 18H_2O + SO_4^{--}$	66.05 [c]	*−6879.31*	*−7846.68*	833.30 [E]	982.61 [E]				316.06 [j]
Thaumasite										
Thaumasite	$CaSiO_3\cdot CaSO_4\cdot CaCO_3\cdot 15H_2O + 3H^+ = 3Ca^{++} + H_4SiO_4 + SO_4^{--} + HCO_3^- + 14H_2O$	10.30[q]	*−7559.67*	*−8682.04*	941.50 [p]	930.00 [p]				329.40

[c] calculated from experiments, this work; [E] estimate, this work; [a] Robie and Hemingway [61]; [b] According to the density obtained by Rinaldi et al. [86]; [d] Warren and Reardon [53]; [f] Berman and Newman [49]; [g] Ederova and Satava [50]; [h] Schoenitz and Navrotski [51]; [i] Moore and Taylor [87]; [j] According to the density provided by Taylor [54]; [k] Houtepen and Stein [43]; [m] Altmaier et al. [68], selection discussed by Blanc et al. [80], [n] Johnson and Glasser [72]; [o] Estimate from Babuskin et al. [42]; [p] Estimate from Schmidt et al. [90]; [q] tentative value as activity and complex formation are neglected in the calculations performed by Macphee and Barnett [89].
Properties in italics have been recalculated using the values in normal characters. Please see online supplementary data for more information.

Table 3
Thermodynamic properties of sulfates and aluminates, collected in the literature.

Mineral	Formula	Log$K$(298)	$\Delta_f G°_{Pr,Tr}$ kJ mol^{-1}	$\Delta_f H°_{Pr,Tr}$ kJ mol^{-1}	$S°_{Pr,Tr}$ J mol^{-1}	Cp(298) J mol^{-1} K^{-1}	a J mol^{-1}	$b*10^3$ J mol^{-1} K^{-2}	$c*10^{-5}$ J mol^{-1} K	Reference
Ettringite	$Ca_6Al_2(SO_4)_3(OH)_{12}\cdot 26H_2O$	57.77	−15,205.74	−17,578.32	1747.24	1794.55	870.27	3100.05		[42]
		56.24	−15,214.46	−17,550.00	1879.42	590.00	590.00			[44]
		56.64								[47]
		57.13								[46]
				−17,539.00						[24]
				−17,544.53						[49]
						2174.36	1939.12	789.00		[50]
		57.74	−15,205.90	−17,535.00	1900.00	2174.24	1939.00	789.00		[6]
Monosulfoaluminate	$Ca_4Al_2(SO_4)(OH)_{12}\cdot 6H_2O$	73.65	−7778.64	−8771.50	747.26	783.68	475.76	1032.78		[42]
		72.25								[46]
				−8778.00						[24]
				−8780.45						[49]
						942.42	594.18	1168.00		[50]
		73.68	−7778.50	−8750.00	821.00	942.24	594.00	1168.00		[6]
Hydrogarnet	$Ca_3Al_2(OH)_{12}$	81.52	−5014.11	−5548.00	404.59	446.96	288.32	532.08		[42,43]
		81.14								[47]
		80.64								[45]
		79.14								[46]
				−5560.54						[49]
						459.35	292.09	561.00		[50]
				−5551.50						[51]
		82.22	−5010.10	−5540.00	419.00	459.26	292.00	561.00		[6]
Gypsum	$CaSO_4\cdot 2H_2O$	4.61	−1797.39	−2022.95	193.80	186.20	186.20			[7]
Anhydrite	$CaSO_4$	4.44	−1322.13	−1434.40	107.40	101.23	102.46	62.88	−17.76	[7]

directly measured by Ederova and Satava [50] and $\Delta_f H°_{P,Tr}$ obtained by Berman and Newman [49] from calorimetry. However, we had to recalculate it in order to take into account $\Delta_f H°_{P,Tr}$ selected here for C3AH6. Indeed, this phase is an element of the thermodynamic cycle used by the authors. Finally, we have obtained $\Delta_f H°_{P,Tr} = -17{,}544.53$ kJ/mol. Fig. 2 allows to verify the agreement between the Log$K(T)$ calculated function and values extracted from selected experiments, as a function of temperature.

3.1.3. Monosulfoaluminate (AFm-SO_4)

In the case of monosulfoaluminate, works published on the solubility of this phase are somewhat sparser. We were not able, as previously, to perform a very strict selection on the basis of the electroneutrality discrepancy of the solutions. Indeed, the authors (Taylor [54], Bennett et al. [52] and Ghorab et al. [5]) do not systematically provide the experimental pH. Only Glasser et al. [41] and Matschei et al. [6] do report measured pHs. In addition, these groups of author have performed long experiments (134 days for Glasser et al. [41] and 450 days for Matschei et al. [6]) and both observe a non congruent dissolution. The incongruency is characterised by the presence of ettringite up to 55 °C and 70 °C, respectively. A problem arises from Matschei et al. [6] experiments, since the results lead the authors to consider ettringite as metastable with respect to AFm-SO_4, at room and higher temperatures. However, 25 °C syntheses of ettringite do not produce impurities [2,41,44,47,53] whereas syntheses of AFm-SO_4 produces systematically ettringite and C3AH6 in most cases. This could indicate the metastability of AFm-SO_4 and contradicts Matschei et al. [6] conclusion.

Calorimetry provides us the Cp(T) function [50]. In addition, Berman and Brown [49] have measured the enthalpy of formation. However, their syntheses produced ettringite, gibbsite and carbonates as impurities. The authors do not provide many details about relative amounts of impurities. The presence of ettringite is inferred only by X-ray analyses. The formation enthalpy must then be considered with caution. In order to introduce an additional constraint, we have considered the phases ettringite, monosulfoaluminate and C3AH6. The

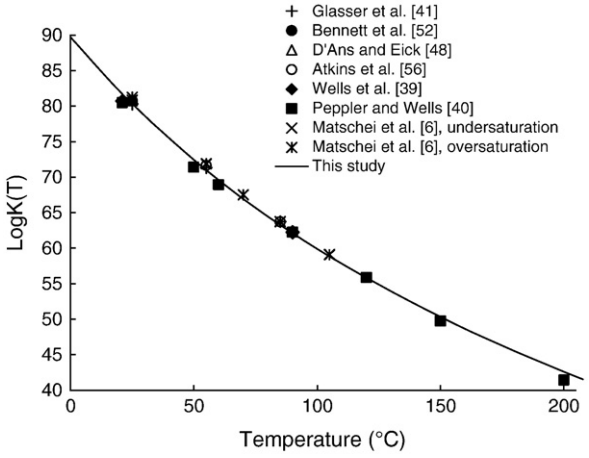

Fig. 1. Equilibrium constant of hydrogarnet C3AH6 as a function of temperature.

Table 4
Selection of experimental data related to the solubility of ettringite at 25 °C.

	Method	Reaction time (days)	Selected compositions	Log$K$ (298)	Standard deviation
Perkins et al. [44]	Dissolution and precipitation	10 to 35	4	57.29[a]	0.16
				56.96[b]	0.28
Ghorab et al. [5]	Dissolution only	14	1	60.28[a] (30 °C)	
Glasser et al. [41]	Dissolution only	151	1	56.88[a]	
				57.68[b]	
Atkins et al. [47]	Dissolution only	14	3	57.08[a]	0.70
Warren and Reardon [53]	Dissolution and precipitation	30 to 60	9	56.97[a]	0.50
				56.97[b]	0.48
Damidot et al. [46]	Dissolution only	56	8	56.79[a]	0.22
Myeni et al. [2]	Dissolution and precipitation	19 21	2	57.30[a]	0.34
				56.60[b]	0.11

[a] Log$K$ calculated from experimental solutions by adjusting pH for electroneutrality.
[b] Log$K$ calculated from experimental solutions without adjusting pH.

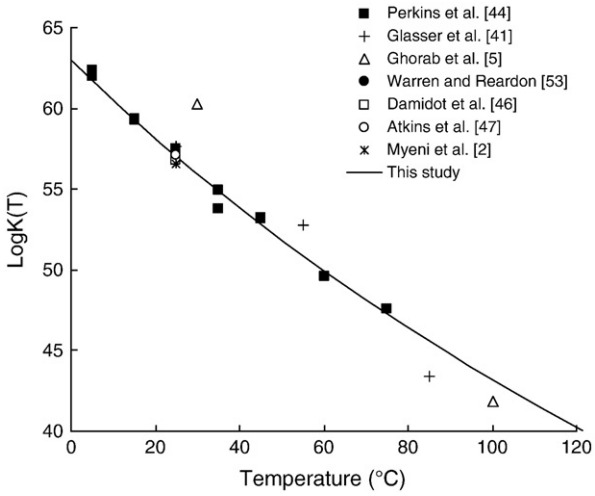

Fig. 2. Equilibrium constant of ettringite as a function of temperature. Except for Ghorab et al. [5] and Glasser et al. [41], only mean values are reported at 25°C, for sake of simplicity.

equilibrium between these three minerals determines an invariant point that depends only on temperature:

$$Ca_6Al_2(SO_4)_3(OH)_{12} : 26H_2O + 2Ca_3Al_2(OH)_{12} = 3Ca_4Al_2(SO_4)(OH)_{12} : 6H_2O + 8H_2O \quad (4)$$

The experiments of Ghorab et al. [5] indicate that this temperature falls between 30 and 100 °C. Damidot et al. [46] have calculated a temperature close to 50 °C for this invariant point. The experimental and analytical work of Stark et al. [55] further confirms the fact that, in Portland cement, ettringite is stable at 25 °C and destabilises at 85 °C. The authors obtained the coexistence of the three phases at 62 °C. Finally, we have retained this temperature for the ettringite–monosulfoaluminate–C3AH6 invariant point, as well as the equilibrium constant extracted from the experiments of Glasser et al. [41] at 25 °C and 85 °C. The minimisation carried out with these three constraints provides an equilibrium constant at 25 °C of Log$K$ = 73.07. The formation enthalpy obtained is −8763.68 kJ/mol, a value intermediate between that provided by Berman and Brown [49] and Matschei et al. [6]. The temperature found for the invariant point is 65 °C.

Finally, Fig. 3 indicates a relatively good agreement between the Log$K(T)$ curve calculated by means of the values selected in this work, with respect to experimental data. However, the stability of the phase may be slightly under-evaluated at high temperature (T>90 °C). In this temperature range it is also possible that monosulfoaluminate is destabilised to the benefit of other sulfates, such as anhydrite. This point will be discussed later on.

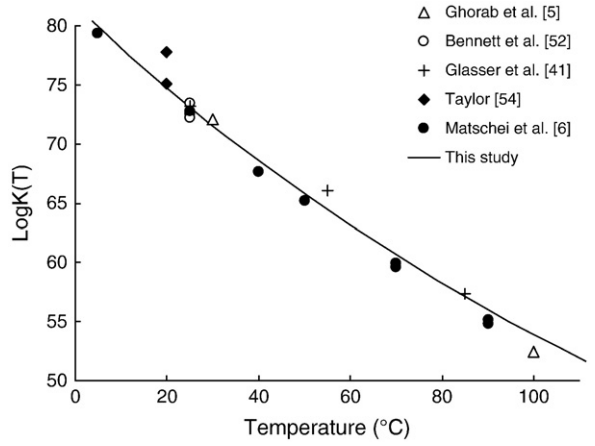

Fig. 3. Solubility of monosulfoaluminate as a function of temperature.

3.1.4. C4AH13 phase (hydroxy-AFm phase)

Since the works of Wells et al. [39] and Peppler and Wells [40], the AFm C4AH13 or C4AH19 phase has been considered unstable at room temperature with respect to C3AH6 and portlandite. Nevertheless, Carlson [58] indicates that C4AH13 may exhibit a thermodynamic stability field at least at T = 1 °C.

As shown by Fig. 4, experimental works concerning the solubility of this phase are actually restrained to a low temperature domain. Indeed, Wells et al. [39] considers that at 21 °C, the assemblage C3AH6 + portlandite replaces C4AH13 + portlandite. If we adopt this hypothesis, the results from Peppler and Wells [40] at 50 °C therefore need to be considered with caution even if their X-ray analyses have confirmed the presence of hexagonal hydrated calcium aluminate among the reaction products. The experiment of Mastchei et al. [6], carried out at 25 °C over 430 days, brings out an essential contribution for the refinement of the equilibrium constant. On the other hand, we have not selected the constant deduced from their experiments in so far as this phase is only present in trace amounts in the final products, confirming Wells et al. [39] statements. Following Wells et al. [39] and Carlson [57], we have considered an intermediate temperature, 11 °C, for the invariant point C4AH13 + C3AH6 + portlandite, which leads to a Log$K$ value of 109.5.

The thermodynamic constants are completed with the enthalpy of formation determined experimentally by Houtepen and Stein [43], −8318.0 ± 8.4 kJ/mol, and a value for Cp(298) obtained by using the estimation technique of Helgeson et al. [37]. Unlike the polyhedral decomposition method [74], it consists in considering a fictive solid–solid transformation reactions like reaction (5), with the hypothesis that Δ_rCp(298) = 0. In the present case, based the following reaction:

$$Ca_3Al_2(OH)_{12} + Ca(OH)_2 + 6H_2O = Ca_4Al_2(OH)_{14} : 6H_2O \quad (5)$$

Cp(298) can then be deduced from portlandite and C3AH6 thermodynamic properties. In addition, we have considered the molecular water under its Ih ice state, whose thermodynamic properties are provided by Mercury et al. [88]. The method also extends to entropy estimates.

In our case, this leads to Cp(298) = 798.90 J/mol K.

We finally obtained the value of 103.65 for the C4AH13 equilibrium constant at 25 °C, slightly smaller than that determined by Matschei et al. [6], namely 104.14. A rather satisfactory agreement may be noted with the experimental data reported in Fig. 4, by calculating the Log$K(T)$ function with selected constants. The experimental points corresponding to Peppler and Wells [40] experiments deviate significantly from the calculated curve. This is not surprising since the association C4AH13 + portlandite is supposed to be unstable at 50 °C.

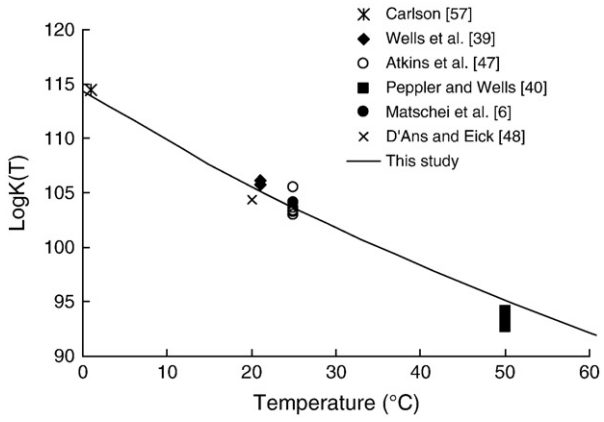

Fig. 4. Equilibrium constant of the AFm C4AH13 phase as a function of temperature.

3.2. System $CaO–Al_2O_3–SiO_2–H_2O$

In this system, three mineralogical families do contain the four components CaO, Al_2O_3, SiO_2 and H_2O: straetlingite ($Ca_2Al_2SiO_3(OH)_8 \cdot 4H_2O$) or hydrated gehlenite, katoite and zeolites. For the latter group, the stability of some of its members will be investigated in Section 4.3.

3.2.1. Straetlingite

Few experiments are available for estimating the equilibrium constant. Among these, the recent experiments performed by Matschei et al. [6] appear by far to be the most relevant. They have used long duration times (up to 84 days), and the electroneutrality discrepancy at 25 °C is small, close to 2.06%. From the solution equilibrated at 25 °C, we extracted a value of Log$K$ = 49.66.

No calorimetric measurements have been published, to date, concerning straetlingite. We then have estimated $S°$ and Cp(298), using Helgeson et al. [37] method with a reaction corresponding to gehlenite hydration toward straetlingite:

$$Ca_2Al_2SiO_2(OH)_{10} : 2.5H_2O = Ca_2Al_2SiO_7 + 7.5H_2O \quad (6)$$

We have retained for gehlenite the properties provided by Robie and Hemingway (1995) ($S°$ = 210.10 J/mol K and Cp(298) = 206.40 J/mol K). Like previously, water is considered under its Ih ice form (properties from Mercury et al. [88]). One then obtains for straetlingite the values $S°$ = 545.88 J/mol K and Cp(298) = 521.48 J/mol K.

We have compared, in Fig. 5, equilibrium constant deduced from literature with the Log$K(T)$ function calculated with previously selected constants. We found a correct agreement with experimental values, even by using previously estimated values for entropy and Cp(298).

3.2.2. Katoite

The name katoite corresponds to a hydrogarnet phase with silica substituting part of the OH groups, with Si<1.5. Indeed, a solid solution develops between the hydrogarnet ($Ca_3Al_2(OH)_{12}$) and grossular ($Ca_3Al_2Si_3O_{12}$) end members [59,60]. No calorimetric study is available for this phase. Concerning solubility data, some papers have been published and are briefly presented in Table 5. Each study deserves some specific comments, in order to enlighten the limits of the experimental conditions. The data presented by Atkins et al. [45] and Bennett et al. [52] are derived from short-term experiments (15 days). Furthermore, among the 4 solution analyses provided by Bennett et al. [52], only one exhibits silica concentration higher than the detection limit, with a discrepancy of the electroneutrality balance close to 30%. The solution composition given by Atkins et al. [45] is provided without measured pH, as for Jappy and Glasser [60] study. Glasser et al. [41] present the longest reaction times (close to one year), with a solution charge imbalance smaller than 2%. But, as they investigated a rather large chemical system, they also obtained portlandite, boehmite and ettringite among the reaction products. A last group of authors, Matschei et al. [6], have performed an interesting set of experiments, at 6 temperatures (from 5 to 85 °C). We found a rather low solution charge imbalance, less than 6%.

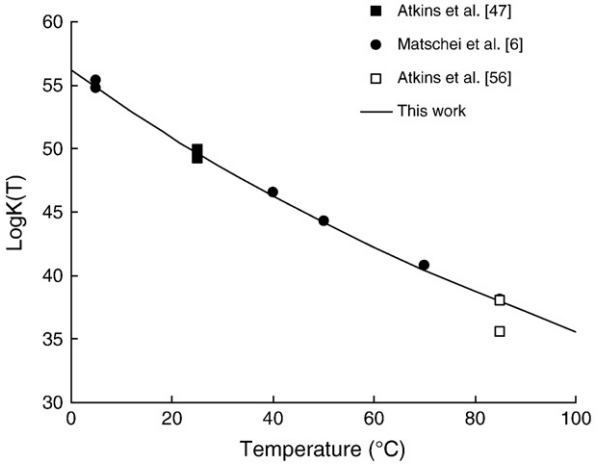

Fig. 5. Temperature dependency of the straetlingite equilibrium constant.

Table 5
Experiments related to katoite equilibration in aqueous media.

Reaction time (days)	Temperature (°C)	Comment	References
15	25	4 solution analyses, 3 analyses with Si<0.01 mmol/l	Bennett et al. [52]
15	25	pH not measured katoite composition not given	Atkins et al. [45]
15	95	pH not measured	Jappy and Glasser [60]
363	25 to 85	Katoite composition from XRD	Glasser et al. [41]
28	5 to 85	3 dispersions in the course of experiments	Matschei et al. [6]

On Fig. 6, we have reported the equilibrium constants derived from 25 °C equilibration experiments, as a function of katoite composition. We observe that equilibrium constants are globally located along the C3AH6–grossular line. However, the dispersion is rather large. The point representing Matschei et al. [6] results at 25 °C falls especially far from the mechanical mixture line. This location is problematic if katoite is considered as a solid solution. It should be noted that the authors have used relatively short reaction time (28 days) In addition, during the course of the experiments, the authors have carried out 3 filtrations/re-dispersions in order to eliminate a residual C–S–H phase. It is possible that the attainment of the equilibrium was perturbed, for kinetic reasons, by this procedure. Such perturbations are also reported for the equilibration of straetlingite by Atkins et al. [45]. Whatever the case, we have adopted for C3ASH4 the value obtained using the solution analysed by Glasser et al. [41], namely 71.16.

We then have used the method of Helgeson et al. [37] to calculate the entropy and the Cp value at 25 °C of the C3ASH4 phase, using the following fictive reaction:

$$Ca_3Al_2SiO_4(OH)_8 = 2/3Ca_3Al_2(OH)_{12} + 1/3Ca_3Al_2Si_3O_{12} \quad (7)$$

We have obtained the values 364.00 J/mol K and 415.07 J/mol K for the entropy and the Cp (298), respectively.

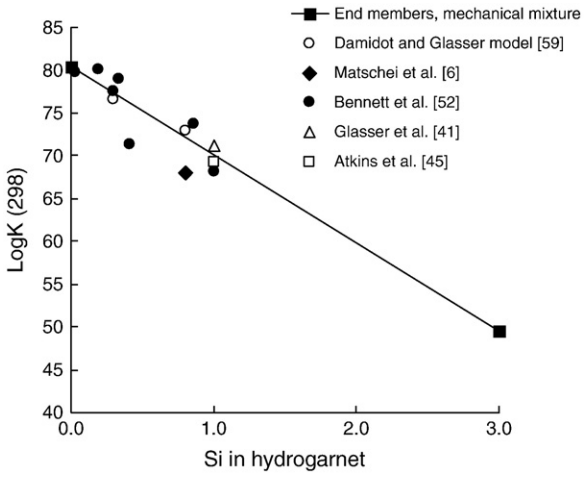

Fig. 6. Equilibrium constants of katoite as a function of composition at 25 °C. End members: hydrogarnet C3AH6 with an equilibrium constant from this study ; grossular (C3ASi3) with an equilibrium constant calculated from Robie and Hemingway [61].

3.3. $CaO–Al_2O_3–CO_2–H_2O$ system

This system is particularly important for the targeted application. It includes phases likely to appear in contact with limestone aggregates and during the carbonation of concrete. It involves monocarboaluminate $3CaO\cdot Al_2O_3\cdot CaCO_3\cdot 10.68H_2O$ and hemicarboaluminate $6CaO\cdot 2Al_2O_3\cdot CaCO_3\cdot Ca(OH)_2\cdot 21H_2O$. The tricarboaluminate phase was proved by Damidot et al. [62] to be unstable with respect to calcite + monocarboaluminate and will not be investigated here. The solubility of monocarboaluminate has been studied by several authors and particularly Damidot et al. [62] and Ghorab et al. [4,5]. Damidot et al. [62] have clearly enlightened the role played by these phases in the carbonation process. These have shown that aluminate C4AH13 is transformed successively into hemicarboaluminate then into monocarboaluminate as the carbonation progresses, the ultimate stage being a mixture of gibbsite and calcite.

The monocarboaluminate equilibrium constant is taken from Damidot et al. [62] experiments because they used longer reaction times than Matschei et al. [6] (180, rather than 84 days, respectively). In addition, the solution composition displays a really low charge imbalance, 1%. The speciation calculation provides a solubility constant of 80.55 for monocarboaluminate, at 25 °C. For hemicarboaluminate, experiments performed by Matschei et al. [6] exhibit the longest reaction times (365 days against 180 for Damidot et al. [62]). Using their 25 °C solution composition, an equilibrium constant is extracted, Log$K$ = 183.70. The enthalpy of formation of monocarboaluminate has been published by Berman and Newman [49]. The value is adjusted for consistency with the formation enthalpy of C3AH6 from Shoenitz and Navrotsky [51], leading to the value −8175.75 kJ/mol. Heat capacity is estimated from the method of Helgeson et al. [37] using the fictive reaction:

$$Ca_4Al_2CO_9 : 10.68H_2O = Ca_3Al_2(OH)_{12} + CaCO_3 + 4.68H_2O \quad (7)$$

We finally obtained Cp(298) = 730.82 J/mol K. We were then able to calculate the evolution of the Log$K(T)$ function as a function of temperature. It displays in Fig. 7 a reasonable agreement with experimental data.

For hemicarboaluminate, no direct measurement is available for entropy, the Cp(T) function nor the enthalpy of formation. Based on values previously found for monocarboaluminate, we have estimated $S°$ and Cp(298) with the Helgeson et al. [37] method applied to the fictive reaction:

$$Ca_8Al_4CO_{16} : 24H_2O + CaCO_3 = 2Ca_4Al_2CO_9 : 10.68H_2O + Ca(OH)_2 + 1.64H_2O \quad (8)$$

We finally found 1269.09 and 1531.53 J/mol K for $S°$ and Cp(298), respectively. With these values, the Log$K(T)$ is calculated in Fig. 8. As for monocarboaluminate, it displays a reasonable agreement with experimental data.

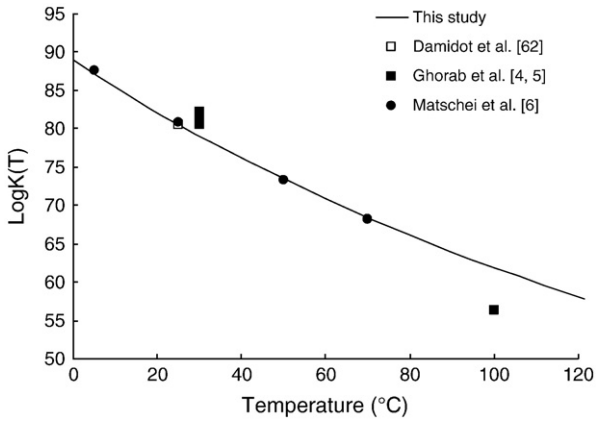

Fig. 7. Equilibrium constant of monocarboaluminate as a function of temperature.

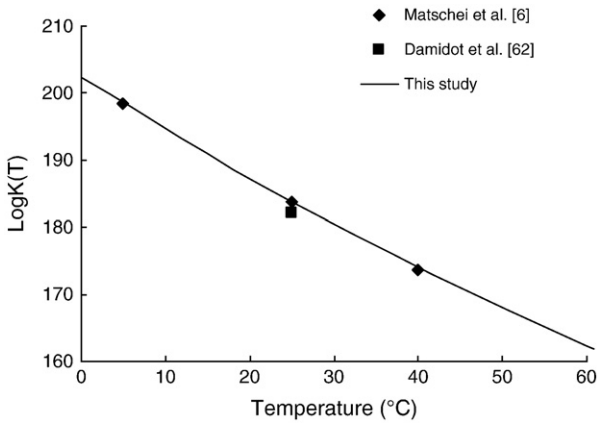

Fig. 8. Equilibrium constant of hemicarboaluminate as a function of temperature.

3.4. Friedel's salt

According to Birnin-Yauri and Glasser [63], the solubility of chlorine is mainly controlled, in cementitious media, by the Cl-AFm, Friedel's salt phase, $2Ca_2Al(OH)_6Cl\cdot 2H_2O$. Birnin-Yauri and Glasser [63] have also pointed out that the Cl-AFt phase could also play a role but, lacking for experimental data, the present selection is restricted to Friedel's salt.

In Fig. 9, we have reported the equilibrium constants derived from experimental studies. At 25 °C, we have retained the value calculated from Glasser et al. [41] solution composition, namely 74.93. It should be noted that they have used reaction times between 1.5 and 2 years, whereas the two other groups of authors have performed the equilibration during 6 months. We favored the experiments that extended over the longest period. In order to calculate the Log$K(T)$ function, we have selected the enthalpy of formation measured by Houtepen and Stein [43], i.e. −7670.04 ± 8.40 kJ/mol. Then, the Cp (298) is estimated by means of the Helgeson et al. [37] method, giving 692.86 J/mol K according to the fictive reaction:

$$2Ca_2Al(OH)_6Cl : 2H_2O = Ca_3Al_2(OH)_{12} + CaCl_2 + 4H_2O \quad (9)$$

In Fig. 9, the agreement with experimental results appears globally correct.

3.5. Magnesium bearing phases

Minerals that control the magnesium concentration in cement pore water are relatively well known [54,65]. Magnesium is

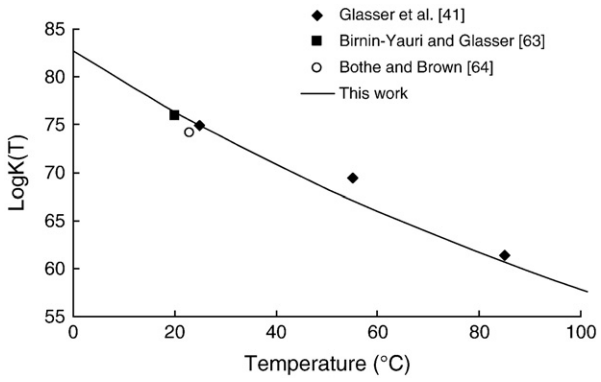

Fig. 9. Friedel's salt equilibrium constant as a function of temperature.

essentially borne by hydrotalcite, a lamellar double hydroxide of aluminium and magnesium, $Mg_4Al_2(OH)_{14}\cdot 3H_2O$ [66]. Brucite Mg $(OH)_2$ can also appear in the hydration products, provided that the Mg/Al ratio of the primary phases is high enough [67].

For the 25 °C equilibrium constant data of brucite, we have considered the recent experiments performed by Altmaier et al. [68], leading to Log$K$ = 17.10. This value is slightly higher than the conventional value of 16.85 published by Nordstrom et al. [69], based on Hostetler [70]. Enthalpy of formation and the Cp(T) function are from Robie and Hemingway [61]. Concerning this phase, Hostetler [70] and Köenigsberger et al. [71] have pointed out that its solubility constant may depend on the surface state of the mineral and its degree of aging.

For hydrotalcite, the data available are more scarce and difficult to use. Bennett et al. [52] have published the composition of 6 solutions equilibrated at 25 °C in the presence of this phase. After speciation calculation, the two solutions with the lowest charge imbalance, <32%, are selected, leading to the mean equilibrium constant Log$K$ = 73.74. To our knowledge, there had not been performed equilibration experiments at higher, to date.

Johnson and Glasser [72] equilibrated a carbonated phase composed by Mg, Al, Ni, Co and Zn. The Mg–Al phase corresponds to the formula $Mg_4Al_2(OH)_{12}(CO_3)\cdot 2H_2O$, it includes a carbonate group. The authors provided its 25 °C equilibrium constant, Log$K$ = 61.19. In order to calculate the complete Log$K$(T) function, we have considered the entropy and heat capacity measured from adiabatic calorimetry by Allada et al. [73] (606.00 and 513.48 J/mol K, respectively), for a $Mg_{4.44}Al_{1.56}(OH)_{12}(CO3)_{0.78}\cdot 2.34H_2O$ phase. We then have applied the Helgeson et al. [37] method to the following reactions:

$$0.78Mg_4Al_2(OH)_{12}(CO_3):2H_2O + 1.32Mg(OH)_2 + 0.78H_2O = Mg_{4.44}Al_{1.56}(OH)_{12}(CO_3)_{0.78}:2.34H_2O \quad (10)$$

$$Mg_4Al_2(OH)_{12}(CO_3):2H_2O + Mg(OH)_2 + H_2O = Mg_4Al_2O_7:10H_2O + MgCO_3 \quad (11)$$

This process finally gives the following values:

- $S°_{Pr,Tr}$ = 512.96 and Cp(298) = 604.15 J/mol K for $Mg_4Al_2(OH)_{12}(CO_3)\cdot 2H_2O$
- $S°_{Pr,Tr}$ = 552.07 and Cp(298) = 556.15 J/mol K for $Mg_4Al_2O_7\cdot 10H_2O$

Lacking of experimental results on the solubility of hydrotalcite at T>25 °C, we are not able to verify the accuracy of the predicted values. In Fig. 10, we have calculated a predominance diagram in the MgO–Al_2O_3–H_2O system as a function of temperature. The brucite stability domain seems to extend to low pH domains as temperature increases.

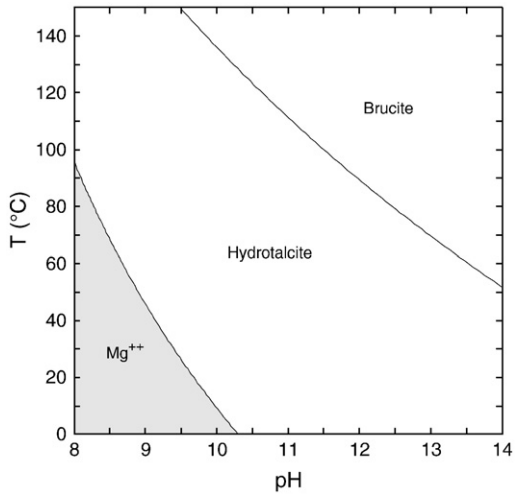

Fig. 10. Stability field of hydrotalcite as a function of temperature in the MgO–Al_2O_3–H_2O system. Total magnesium and aluminum concentrations, $[Al^{++}]_T = [Mg^{++}]_T$ = 0.05 mmol/l.

3.6. Iron bearing phases

Cement pastes contain a non-negligible proportion of ferric iron. During hydration, several minerals may incorporate it. As shown by Schwarz [75], Emanuelson and Hansen [76], Csizmadia et al. [77] and Rose et al. [79], iron may replace aluminium in AFm type phases (C4AH13 and monosulfoaluminate, particularly), in hydrogarnet and even in ettringite. However, an ambiguity remains concerning the stability or the metastability of iron bearing phases in cementitious media. Emanuelsson and Hansen [76] have observed, during the hydration of C4AF at 20 °C in pure water, amorphous AFm phases containing a high proportion of iron, evolving towards hydrogarnet as hydration progressed. In the presence of gypsum, they have concluded that the AFm phase destabilises over time to form ettringite. On the other hand, Rose et al. [79] have concluded, from XAS synchrotron experiments, that C4AF hydration produces a mixture of C3FH6 and an amorphous FeOOH phase. In the present discussion, we only considered those iron bearing phase whose presence had been discussed in previous studies.

Until very recently, the only known thermodynamic properties for those iron bearing phases consisted in estimates published by Babushkin et al. [42]. In a recent publication, Moschner et al. [78] propose a whole series of experiments concerning the solubility of ettringite-Fe, monosulfate-Fe and monocarbonate-Fe. Those long-term (up to 180 days) experiments are carried out from both under and supersaturation. From the solution compositions, we have re-evaluated the equilibrium constants, for sake of consistency with our main database. We only retained the composition corresponding to experiments with charge imbalance smaller than 5%. We have obtained the following equilibrium constants at 20 °C:

- −45.15 for ettringite-Fe instead of −44.0 ± 0.7 [78]
- −33.24 for monosulfate-Fe instead of −33.2 ± 0.7 [78].

The main discrepancy with Moschner et al. [78] concerns ettringite-Fe. It arises from the selection of solution compositions, as explained before. Monocarbonate-Fe could not be considered here since we are using the Debye–Hückel activity model and the lowest ionic strength is 0.37.

In order to obtain the full set of thermodynamic constants, we have estimated the entropies and heat capacities of these phases, using the method of Helgeson et al. [37]. We have considered fictive solid–solid reactions involving ettringite and monosulfoaluminate:

$$Ca_6Al_2(SO_4)_3(OH)_{12}:26H_2O + 2FeOOH = Ca_6Fe_2(SO_4)_3(OH)_{12}:26H_2O + 2AlOOH \quad (12)$$

$$Ca_4Al_2(SO_4)(OH)_{12}:6H_2O + 2FeOOH = Ca_4Fe_2(SO_4)(OH)_{12}:6H_2O + 2AlOOH \quad (13)$$

The reactions have been equilibrated with boehmite and goethite. The boehmite/goethite (AlOOH/FeOOH) pair was preferred to the gibbsite/ferrihydrite ($Al(OH_3$/$Fe(OH)_3$) pair due to large uncertainties on the entropy and the heat capacity of ferrihydrite. The results are presented in Table 6.

In addition, we have tried to refine the thermodynamic properties of C3FH6 and C4AH13. We selected the only $\Delta_f H°_{P_r,Tr}$ available, from Babushkin et al. [42] estimates. Then $S°_{P_r,Tr}$ and Cp(298) were estimated using Helgeson et al. [37] and the following reactions:

$$C3AH6 + 2FeOOH = C3FH6 + 2AlOOH \quad (14)$$

$$C4AH13 + 2FeOOH = C4FH13 + 2AlOOH \quad (15)$$

The results are given in Table 6 which also provides a comparison with previously published values, from Moschner et al. [78] and Babushkin et al. [42]. Sulfate properties derived here are close to that

Table 6
Data used in the calculation of thermodynamic properties of iron bearing phases, comparison with literature data.

Minerals	$\Delta_f H^\circ_{Pr,Tr}$ kJ mol^{-1}	$S^\circ_{Pr,Tr}$ J mol^{-1} K^{-1}	Cp(298) J mol^{-1} K^{-1}	References
Ettringite	−17,544.53	1883.59	2174.36	This work
Monosulfoaluminate	−8763.68	786.94	942.42	This work
C3AH6	−5551.50	416.61	459.35	This work
C4AH13	−8318.00	685.13	798.90	This work
Boehmite, AlOOH	−996.40	37.20	54.24	Blanc et al. [80]
Goethite, FeOOH	−559.12	60.40	74.33	Grivé [81]
Ettringite-Fe	−16,601.22	1930.11	2214.54	This work
	−16,600.00	1937.00	2200.00	Moschner et al. [78]
Monosulfate-Fe	−7846.68	833.30	982.61	This work
	−7843.00	858.00	968.00	Moschner et al. [78]
C3FH6	−4647.59	436.84	484.15	This work
	−4647.59	424.66	486.43	Babushkin et al. [42]
C4FH13	−7417.40	705.35	787.08	This work
	−7417.40	738.06	981.86	Babushkin et al. [42]

obtained by Moschner et al. [78], especially for ettringite. On the other hand, our estimate of the entropy and heat capacity of C4FH13 are lower than Babushkin et al. [42] values, which would decrease the C4FH13/C3FH6 transition temperature, in our case.

3.7. Thaumasite

Thaumasite is a complex silicate phase whose chemical formula corresponds to $CaSiO_3 \cdot CaSO_4 \cdot CaCO_3 \cdot 15H_2O$. It is expected to be stable in low temperature systems, usually less than 20 °C ([89], [90]). This temperature domain is rather low for deep disposal concerns but since this phase seems to be frequently implied into concrete degradation processes [90], we have included it into the present selection. Its solubility has been investigated namely by Macphee and Barnett [89] and reinterpreted latter by Schmidt et al. [90]. Macphee and Barnett [89] experiments represent the most complete source of data for assessing thaumasite solubility. However, because the synthesis process always produces a mixture of phases belonging to the thaumasite–ettringite series, the interpretation of the solubility experiment involves using a solid solution approach. We are relying on the equilibrium constants deduced by Macphee and Barnett [89] that way, which are reported in Fig. 11. This figure also displays an equilibrium constant deduced by Damidot et al. [91] and the Log$K(T)$ curve deduced by Schmidt et al. [90] from [89] experimental data. The discrepancy observed could arise partially from the pH assessment, since it is not measured experimentally [89]. It could also result from applying an ettringite–thaumasite solid solution model [89]. This is probably the main explanation because in considering only pH corrected from electroneutrality, we could get similar results than Schmidt et al. [90]. Selecting Schmidt et al. [90] estimate for entropy and Cp(298), respectively 941.50 and 930.00 J/mol K, we could obtain the 25 °C equilibrium constant (see Table 2) from the 15 °C experiments since thaumasite is supposed to be stable in this temperature range [89]. The resulting Log$K(T)$ function is displayed in Fig. 11. Uncertainties remain concerning thaumasite thermodynamic properties, its 25 °C equilibrium constant is indeed a tentative value as activity and complex formation has been neglected in the calculations performed by Macphee and Barnett [89]. In addition, we are lacking for a synthesis experiment without secondary products and a solution analysis without calculated parameters or concentrations under the detection limits in order to get a more precise determination. Because of its complex chemical composition, testing its phase relations is not straightforward and predominance diagrams are not the more convenient tool for this task. Geochemical modelling is usually preferred [90] but it is not considered in the present work.

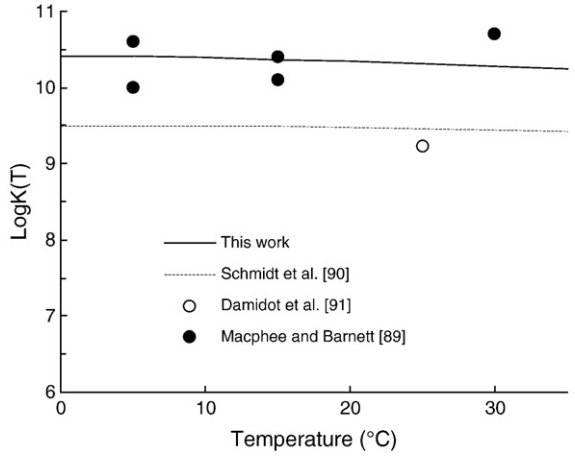

Fig. 11. Thaumasite equilibrium constant as a function of temperature.

4. Discussion: predominance diagrams

The selection of thermodynamic constants allows to realise predominance diagrams in different chemical sub systems, as a function of temperature. Such diagrams are first drawn in order to verify the predicted phase relations. They may be of help when no other data are available and they are also helpful for understanding the temperature and composition effects on mineral stability ranges. However, the verification process mainly relies on the location of invariant points. The diagrams are not directly of use to predict the solution composition of actual cementititous systems in the other cases. Indeed, in actual cement systems, phase boundaries may be influenced through interactions between sub systems or because of the presence of external elements, like alkalis for instance.

4.1. System $CaO–Al_2O_3–SO_3–CO_2–H_2O$

Predominance diagrams for the systems $CaO–Al_2O_3–H_2O$ and $CaO–Al_2O_3–SO_3–H_2O$, including the temperature dependency, are represented in Figs. 12–14. Fig. 12 shows that, in the presence of portlandite and C3AH6, monosulfoaluminate is stable between 65 and 121 °C. It is then transformed into ettringite + C3AH6 when $T<65$ °C and into anhydrite + C3AH6 when $T>121$ °C.

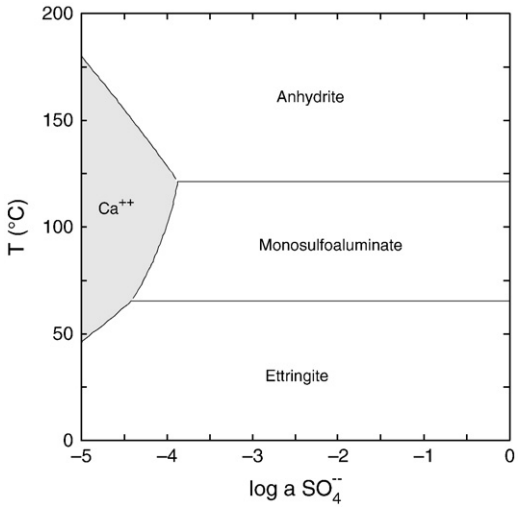

Fig. 12. Phase relations in the system $CaO–Al_2O_3–SO_3–H_2O$, as a function of temperature. The solution is saturated with respect to portlandite and C3AH6.

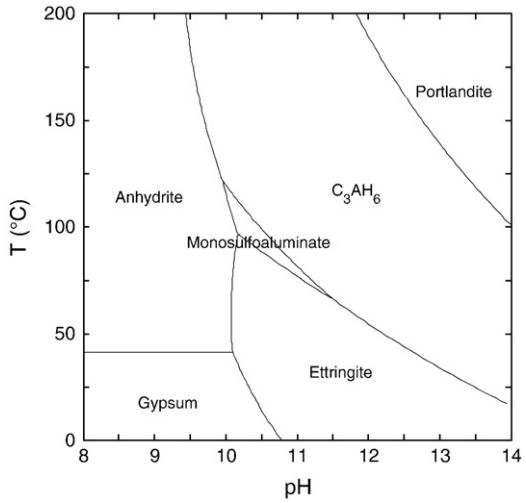

Fig. 13. Phase relations in the system $CaO–Al_2O_3–SO_3–H_2O$, as a function of temperature. The solution is saturated with respect to gibbsite and $[SO_4^{--}]_T = 1$ mmol/l.

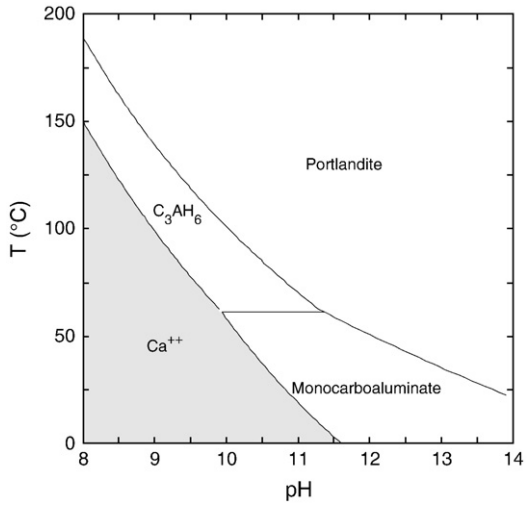

Fig. 15. Phase relations in the system $CaO–CO_2–Al_2O_3–H_2O$ as a function of temperature. The solution is saturated with respect to calcite and $[Al^{+++}]_T = 0.1$ mmol/l.

On the other hand, Fig. 13 also shows that, in the presence of anhydrite, the monosulfoaluminate/ettringite transition takes place at 96 °C. In addition, it indicates that phase relations between ettringite and monosulfoaluminate do not depend only on temperature as both phases are not strictly polymorphs. This issue, already pointed out by Damidot and Glasser [48] and Bothe and Brown [64], namely, explains that a precise transition temperature cannot be given. In addition, phase relations drawn in Fig. 13 may be modified because of the influence of solid solutions [6] and of kinetic factors. This diagram also indicates that the lowest temperature of formation for monosulfate corresponds to the appearance of the invariant point with ettringite and C3AH6, as already stated by Damidot and Glasser [46]. They had found $T = 50$ °C for the invariant, not far from the 65 °C found here.

For aluminate phases, the diagram presented in Fig. 13 shows that the transition temperature between C4AH13 and C3AH6 varies as a function of the Al(OH)4-/OH^- activity ratio, the highest temperature being reached when the solution becomes saturated with respect to portlandite (invariant point at 11.7 °C).

It may be noted in Fig. 15, that at 25 °C and in the presence of calcite and portlandite, the appearance of monocarboaluminate is incompatible with that of C3AH6. At 63 °C, the invariant point corresponds to the simultaneous appearance of the four phases and to the maximum temperature extent for the monocarboaluminate stability field. These results are similar to those obtained by Damidot et al. [62]. It also means that calcite may be at equilibrium with portlandite and monocarboaluminate, even in alkaline solutions. This enhances the long-term compatibility of carbonate (calcite) aggregates in cement systems.

4.2. System $CaO–Fe_2O_3–SO_3–H_2O$

Predominance diagrams have been drawn for chemical system similar to the previous case, but replacing Al_2O_3 by Fe_2O_3. These are reported in Figs. 16 and 17. These figures indicate that the phase relations are similar to that in the $CaO–Al_2O_3–SO_3–H_2O$ system, except for the stability field of monosulfate-Fe that extends to the room temperature, in agreement with Moschner et al. [78] results. The diagram would indicate that iron enhances the stability of AFm-SO_4 at low temperatures, whereas it decreases the pH stability domain of ettringite.

In addition, the diagram represented in Fig. 17 indicates phase relations and transition temperatures between C4FH13 and C3FH6 which are similar to the aluminate case. The C4FH3–C3FH6–portlandite invariant point is found at 26 °C, which is close to the 21 °C found by Rogers and Aldridge [85] for the C4(A, F)H13 to C3(A, F)H6 conversion. It must be pointed out that, without the modifications to Babushkin et al. [42] estimates for $S°_{P_r,Tr}$ and Cp(298) of C4FH13 and C3FH6, the invariant

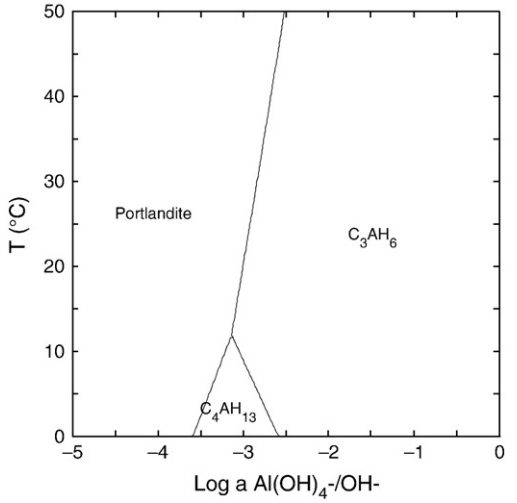

Fig. 14. Phase relations in the system $CaO–Al_2O_3–H_2O$ as a function of temperature. Total calcium concentration $[Ca^{++}]_T = 10$ mmol/l.

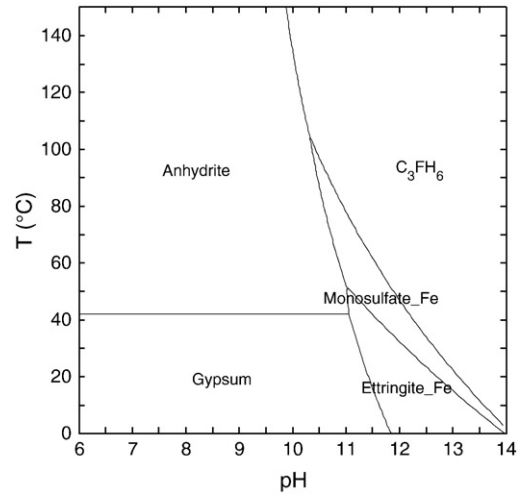

Fig. 16. Phase relations in the system $CaO–Fe_2O_3–SO_3–H_2O$ as a function of temperature. The solution is saturated with respect to ferrihydrite and $[Ca^{++}]_T = 10$ mmol/l.

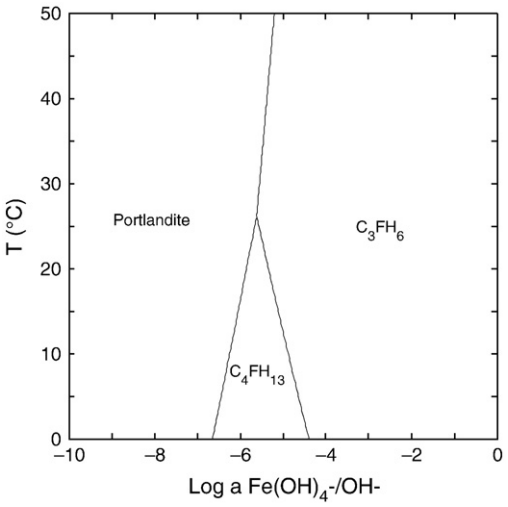

Fig. 17. Phase relations in the $CaO–Fe_2O_3–H_2O$ system as a function of temperature. Total calcium concentration $[Ca^{++}]_T = 10$ mmol/l.

point temperature would be shifted to 85 °C which strongly contradicts literature results where C3FH6 is found to be stably close to room temperature [59,85].

In any cases, phase relations displayed here do need some experimental assessment from additional experimental work, especially concerning C4FH13 and C3FH6.

4.3. System $CaO–Al_2O_3–SiO_2–H_2O$

This system includes mineral phases important for cementitious material, straetlingite, katoite, C–S–H and zeolites. Except for C–S–H, few constraints allow to determine their stability domains. Predominance diagram bring an alternative way to discuss such phase relations.

This discussion is based on C–S–H properties already refined by Blanc et al. [1]. For zeolites, we have considered the review proposed by Blanc [82]. The case of zeolite-CaP is discussed here.

4.3.1. Katoite

Fig. 18 represents phase relations in the $CaO–Al_2O_3–SiO_2–H_2O$ system, at 25 °C, based on our selection of thermodynamic properties. It appears that the equilibrium constant selected for katoite forbids C3AH6 to reach the equilibrium with portlandite and CSH1.6. As shown by Damidot and Glasser [59], the katoite phase at equilibrium with C–S–H and portlandite should be enriched by silica as temperature increases, starting with a C3AH6 phase substituted by 0.3 Si at 25 °C. In our case, we have calculated that the katoite equilibrium constant must be above $LogK = 71.8$ in order to allow C3AH6 to be at equilibrium while the selected value at 25 °C is $LogK = 71.16$. We have also calculated that a mechanical mixture between C3AH6 and grossular end members would result in $LogK = 70.06$, indicating a higher stability than previous values. From Ganguly and Saxena [83] this case would appear only inside a solvus zone (miscibility gap) and it would indicate that the phase is metastable. From Jappy and Glasser [60] study, Damidot and Glasser [59] indicate a solubility gap between 0.3 and 0.8 Si. Considering a regular solid solution model would lead to an end member having 1.1 Si, far from hibschite composition (1.5 Si). By defining a high solubility for this phase, we could overcome the preceding question. But, up to date, we have no evidence for such a solubility. We had previously underlined the difficulties in selecting thermodynamic properties of katoite. We must admit that selected values do not allow to completely describe the phase relations with other minerals. A solid solution model could be employed, provided that composition and stability of the silica rich end member are clarified. To our knowledge, the available experimental data are not sufficient to provide a more precise selection. We retain the properties selected here for katoite, as tentative values.

4.3.2. Zeolite-CaP

This phase is directly related to the mineralogy of blended, Al rich cements [58], like chabazite [56]. Its crystalline structure is close to that of gismondine.

Atkins et al. [56] have equilibrated a synthetic, CaP sample, at both 25 and 85 °C. But the composition of the solutions is reported without silica concentration. The electroneutrality discrepancy of the solutions is close to 30% at 25 °C. It is difficult to make use of these results. However phase relations highlighted in predominance diagrams can help us to estimate a reasonable value for the equilibrium constant. If we consider that straetlingite is stable at least at 25 °C, according to Atkins et al. [56], it would be in equilibrium with a C–S–H of low C/S ratio (but higher than 1 [56]) and katoite [56]. In our case, we consider the CSH1.2 phase (C/S = 1.2). From Fig. 18, the preceding conditions imply an equilibrium constant ranging from 43.3 and 47.0. We retain the intermediate value, $LogK = 45.15$.

At 85 °C, Atkins et al. [56] indicate that straetlingite becomes metastable with respect to the assemblage katoite/zeolite-CaP/gibbsite (see Fig. 19). This condition sets the equilibrium constant at $LogK = 28.07$. The Van't Hoff relation then enables to calculate the

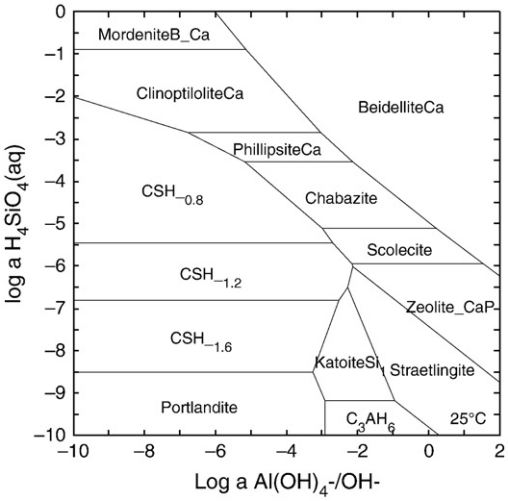

Fig. 18. Stability domain of zeolite-CaP at 25 °C. Total calcium concentration $[Ca^{++}]_T = 10$ mmol/l.

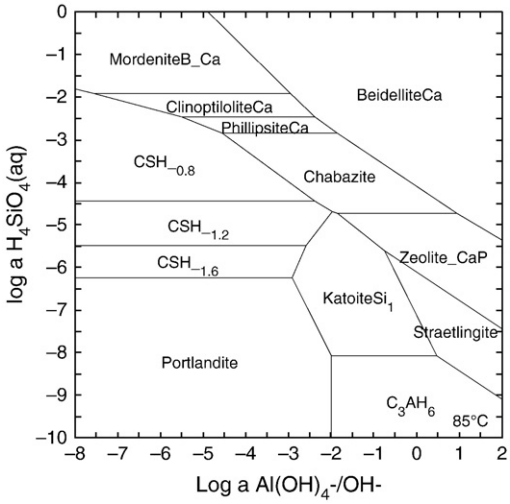

Fig. 19. Stability domain of zeolite-CaP at 85 °C. Total calcium concentration $[Ca^{++}]_T = 10$ mmol/l.

reaction enthalpy, i.e. −527.74 kJ/mol and the enthalpy of formation, −11,129.11 kJ/mol.

The whole diagram displayed in Fig. 18 is globally consistent with previous calculations made by Damidot and Glasser [59]. Considering that the activity of dissolved silica decreases as the pH decreases, the sequence of minerals found from the bottom to the top of the figure may represent the mineralogical transformations occurring during a meteoric alteration. Savage et al. [84] have reviewed the main mineralogical transformations expected during cement alteration. In the $CaO–Al_2O_3–SiO_2–H_2O$ system, they underline especially the progressive loss of calcium in C–S–H phases and the silica enrichment in zeolites, as meteoric degradation proceeds, which is consistent with the diagram drawn in Fig. 18. From Figs. 18 and 19, it appears that the stability domain of katoite increases with temperature, as expected.

4.4. AFm and hydrogarnet: phase relations from simple chemical systems to actual cement

Phase relations between hydrogarnet-like and AFm phases remains a recurring matter of discussion. We have tried here to synthesize the main features concerning this matter, in relation with the properties refined and illustrated in the present work.

From what precedes, it is clear that the phase relations between hydrogarnet and AFm phases are related namely to chemical parameters and temperature. We are going to discuss these points, starting by the simplest chemical system, $Al_2O_3–CaO–H_2O$. Considering the $Al_2O_3–CaO–H_2O$ system, it has long been established that C_3AH_6 is the stable phase at near room temperature while C_4AH_{13} (the AFm phase) is stable at lower temperatures [6,39,40,57]. Fig. 14 is in agreement with this statement. Actually, experiences from Peppler and Wells [40] indicate the presence of C_4AH_{13} even at 50 °C but the calculation of the IAP from solution analyses displays undersaturation with respect to the equilibrium constant (see Fig. 4). At 50 °C, the equilibrium of C4AH13 with solution is thus metastable, it begins to undergo a conversion to C3AH6 that takes place gradually, which explains why amounts of C4AH13 can still be detected by X-ray diffraction [40]. The addition of sulfates complicates the system by extending the stability field of AFm toward higher temperatures (Fig. 12) and by adding the AFt phases to the system. It also determines an invariant point for the monosulfate (AFm)–ettringite (AFt)–C3AH6 assemblage, corresponding to reaction (4). In this reaction the stoichiometric coefficient of water is different from zero, so that this assemblage is no longer an invariant when the water activity is lower than 1. In water, we have previously discussed the fact that the invariant point seems to lie between 25 and 90 °C, rather close to 60 °C. A more precise temperature determination is still lacking. But recent investigations [92] indicate that during a temperature increase from 25 °C up to 250 °C in 2 h, ettringite evolves into monosulfate plus bassanite, between 115 and 120 °C, while monosulfate is replaced by C3AH6 plus bassanite/anhydrite between 170 to 220 °C. The transition temperature between monosulfate and ettringite is close to that found in Fig. 13, considering that the latter is drawn with anhydrite instead of bassanite. We could calculate that replacing anhydrite by bassanite would lead to a transition temperature of 111 °C, closer to the experimental results [92]. On the other hand, the formation of C3AH6 begins with the gradual disappearance of monosulfate from 170 to 220 °C and the nucleation of C3AH6 starting from 210 °C. From the data refined in this study (Table 2), we have calculated a temperature of 152 °C for the C3AH6–monosulfate–bassanite triple point whereas it is obtained experimentally close to 210 °C [92]. Since the temperature of the previous triple point was rather correctly predicted, the discrepancy would arise from C3AH6 properties. We could calculate that a displacement of the invariant point from 152 to 170 °C would lead to destabilise the 25 °C Log*K* by 0.5 which is still compatible with the dispersion in Fig. 1. The discrepancy would reach 1.5 if one considers 210 rather than 170 °C. This is no longer compatible with Fig. 1. Considering that 170 °C is the most probable experimental temperature for the invariant point, the temperature based on data refined in this study, 152 °C, appears rather compatible with experimental results. The appearance of crystalline C3AH6 would be delayed because of kinetic constraints, as previously stated.

Up to now, we have considered that the water activity equals to 1, meaning that the system is fully saturated, which is actually the case in disposal conditions. A water activity lower than 1 is an interesting case, namely for meteoric alteration. Albert et al. [93] have calculated that, at room temperature, the assemblage ettringite–monosulfate–C3AH6 would be in equilibrium with a relative humidity of 66, 69 or 98% depending on the thermodynamic database. In fact, the last case is obtained by using Babushkin et al. [42] database and could be somewhat less probable. Applying the same calculation process with data from Tables 1 and 2, we obtained a relative humidity of 64% which is rather satisfactory. In all cases, ettringite is favored by high water activities, as it is the case in saturated disposals.

In addition to sulfate or the relative humidity, carbonates have a strong influence on those phase relation [94]. Even a small amount of carbonates would induce to transform monosulfoaluminates into monocarbonate [94]. In that case, monosulfate could disappear but, monocarbonate being an AFm phase, the latter would be strongly stabilized, which is also illustrated in Fig. 15.

Influence of iron is rather difficult to assess, even for the simple system $CaO–Fe_2O_3–H_2O$. Indeed, in this work, the thermodynamic properties of C4FH13 and C3FH6 are only broadly constrained by estimate calculation. Results obtained by Collier et al. [95] seem to indicate that iron is stabilizing the hydrogarnet phase, even at 20 °C. The phase relations calculated here and displayed in Fig. 17, are not very different from what can be obtained for the $CaO–Al_2O_3–H_2O$ system. The discrepancy with experiments [95] may arise either from uncertainties in the estimate calculation or because the presence of iron may favor the precipitation of the cubic phase, from a kinetic point of view. Collier et al. [95] also indicate that iron would also favor the monosulfate over ettringite, in agreement with Fig. 16.

Silica substitution is also involved in AFm–hydrogarnet phase relations, by extending the stability field of C3AH6 as reported by de Sylva and Glasser [96]. In experiments performed on metakaolin–lime systems, katoite was observed by XRD and DTA only at 55 °C, with a Si substitution ranging from 0.26 to 0.90, depending on starting compositions. In addition, 2 AFm phases were obtained, C4AH13 and C2ASH8, with the amount of C4AH13 decreasing with curing time, even at 20 °C. In other terms, Si substitution would stabilize hydrogarnet and also AFm phases with the appearance of C2ASH8. Mc Dowell [97] have also considered the chemical system $CaO–SiO_2–Al_2O_3–H_2O$ but with a more reactive starting material, that is glass cement instead of metakaolin–lime mixtures. After hydration at room temperature, the paste is then composed either by stratlingite or katoite or a mixture [97]. In glass cement, the elements release is quickest, less dependent on the dissolution path and the equilibrium is supposed to be reached more quickly. Stratlingite and katoite are thus probably the stable phases at room temperature, depending on initial mixture compositions. However, the results from de Siva and Glasser [96] indicate that katoite precipitation is clearly more dependent on kinetic factors.

The ancient constructions bring out examples of long-term evolution of cementitious materials [98]. For example, Rassineux et al. [99] have analysed and characterised hydrogrossular with various extent of the Si substitution, in mortars from Roman Thermal Baths. In ancient mortars, monosulfate is very rare (in fact not reported, to our knowledge), contrary to ettringite [98,99]. Because ettringite equilibrates with a higher sulfate concentration than monosulfate [100], this could be the consequence namely of a sulfate leaching that would re-concentrated near the solid–air interface. But the interpretation will become more complex by taking into account the influence of the relative humidity or

other chemical elements like iron, chloride or carbonates. In addition, not only katoite but also zeolites could represent stable phases [101] as previously observed at 20 °C for fly ashes cement [102].

Finally, we can established that in chemical systems involving AFm and hydrogarnet phases, the phase relations calculated here seem rather correct with respect to experimental works, for simple, reduced chemical system at least. However, for actual cement systems we have to consider some more complex phase relations. For example, if monosulfate is very rare in ancient mortars, AFm phases may still be stable, depending on the available amounts of silica, carbonates, iron or chloride. In addition, all the phase diagrams displayed here are based on equilibrium thermodynamics whereas kinetic constraints seem to play a major role in hydrogrossular precipitation. Finally, even if phase relations calculated here for simple chemical systems seem to be correct, contradictory observations may arise from the influence of additional chemical elements or from kinetic factors.

5. Conclusion

The aim of this work was to provide thermodynamic constants in order to calculate the equilibrium constants of minerals that characterize cementitious media, as a function of temperature. In most cases, the dataset has to be completed by estimated values. Globally, we have been able to check the consistency of the selection by drawing predominance diagrams for each chemical sub system investigated.

Considering the selection itself, the main source of uncertainty arise from equilibration experiments. The collection of experimental data has allowed to highlight namely the importance of reaction times. The charge imbalance of the solutions has also been used as a selection criterion because discrepancies may come from analytical problems or from chemical elements external to the system of interest.

Some rather consistent phase relations have been obtained for the SO_3–Al_2O_3–CaO–CO_2–H_2O system. The addition of iron III enlarges the AFm–SO_4 stability field to the low temperature domain, whereas it decreases the pH domain where ettringite is stable. On the other hand, the stability field of katoite remains largely ambiguous, namely with respect to a solid solution hydrogarnet/grossular.

Finally, predominance diagrams help in discussing the chemical compatibility of aggregates with cement pastes, within the context of long-term, deep disposals.

Acknowledgements

This study was financially supported by ANDRA (Thermochimie Project) and BRGM (Project PDR07EPI54). An anonymous reviewer is acknowledged for fruitful comments and suggestions that contributed strongly to improve the document. We especially thank Colin Walker in helping to correct the diagrams and Karen Scrivener for her support.

Appendix A. Supplementary data

Supplementary data associated with this article can be found, in the online version, at doi:10.1016/j.cemconres.2010.04.003.

References

[1] P. Blanc, X. Bourbon, A. Lassin, E.C. Gaucher, Chemical model for cement-based materials: thermodynamic data assessment of amorphous and crystalline C-S-H phases, Cem. Concr. Res. 40 (2010) 851–866.
[2] S.C.B. Myneni, S.J. Traina, T.L. Logan, Ettringite solubility and geochemistry of the Ca $(OH)_2$ – $Al_2(SO_4)_3$–H_2O system at 1 atm pressure and 298 K, Chem. Geol. 148 (1998) 1–19.
[3] R.B. Perkins, C.D. Palmer, Solubility of ettringite $(Ca_6[Al(OH)_6]_2.(SO_4)_3 26H_2O)$ at 5–75 °C, Geochim. Cosmochim. Acta 63 (1999) 1969–1980.
[4] H.Y. Ghorab, E.A. Kishar, S.H.A. Elfetouh, Studies on the stability of the calcium sulfoaluminate hydrates. Part II: effect of alite, lime, and monocarbonaluminate hydrate, Cem. Concr. Res. 28 (1998) 53–61.
[5] H.Y. Ghorab, E.A. Kishar, S.H.A. Elfetouh, Studies on the stability of the calcium sulfoaluminate hydrates. Part III: the monophases, Cem. Concr. Res. 28 (1998) 763–771.
[6] T. Matschei, B. Lothenbach, F. Glasser, Thermodynamic properties of Portland cement hydrates in the system CaO–Al_2O_3–SiO_2–$CaSO_4$–$CaCO_3$–H_2O, Cem. Concr. Res. 37 (2007) 1379–1410.
[7] P. Blanc, P. Piantone, A. Lassin, A. Burnol, Thermochimie: Sélection de constantes thermodynamiques pour les éléments majeurs, le plomb et le cadmium, Rapport final: BRGM RP-54902-FR, 2006.
[8] P. Piantone, C. Nowak, P. Blanc, A. Lassin, A. Burnol, Themoddem: THERmodynamique et MOdélisation de la Dégradation DEchets Minéraux, Rapport d'avancement. BRGM n° BRGM/RP- 54547-FR, 2006 http://thermoddem.brgm.fr/.
[9] J.D. Cox, D.D. Wagman, V.A. Medvedev, CODATA Key Values for Thermodynamics, New York Hemisphere Publishing Corporation, 1989.
[10] V.A. Pokrovskii, H.C. Helgeson, Thermodynamic properties of aqueous species and the solubilities of minerals at high pressures and temperatures: the system Al_2O_3–H_2O–NaCl, Am. J. Sci. 295 (1995) 1255–1342.
[11] D.J. Rimstidt, Quartz solubility at low temperatures, Geochim. Cosmochim. Acta 61 (1997) 2553–2558.
[12] H. Wanner, Guidelines for the review procedure and data selection, NEA TDB-1 Guidelines (http://www.nea.fr/html/dbtdb/guidelines) (2000).
[13] I. Grenthe, H. Wanner, Guidelines for the extrapolation to zero ionic strength, NEA TDB-2 Guidelines (http://www.nea.fr/html/dbtdb/guidelines) (2000).
[14] I. Puigdomenech, J.A. Rard, A.Y. Plyasunov, I. Grenthe, Temperature corrections to thermodynamic data and enthalpy calculations, NEA TBD-4 Guidelines (http://www.nea.fr/html/dbtdb/guidelines) (1999).
[15] H.C. Helgeson, D.H. Kirkham, G.C. Flowers, Theoretical prediction of the thermodynamic behavior of aqueous electrolytes at high pressures and temperatures: IV. Calculation of activity coefficients, osmotic coefficients, and apparent molal and standard and relative partial molal properties to 600 °C and 5 kbar, Am. J. Sci. 281 (1981) 1249–1516.
[16] D.L. Parkhurst, C.A.J. Appelo, PHREEQC 2: a Computer Program for Speciation, Batch-Reaction, One-Dimensional Transport and Inverse Geochemical Calculations, USGS, Denver, 2001.
[17] C.M. Bethke, The Geochemist's Workbench® Release 6.0 — Reference Manual, University of Illinois, 2006.
[18] M.W.J. Chase, NIST-JANAF Thermochemical Tables: National Institute of Standards and Technology, fourth edition, J Phys Chem Ref Data, 9, 1998.
[19] M.D. Schulte, E.L. Shock, R.H. Wood, The temperature dependence of the standard-state thermodynamic properties of aqueous nonelectrolytes, Geochim. Cosmochim. Acta 65 (2001) 3919–3930.
[20] E.L. Shock, H.C. Helgeson, Calculation of the thermodynamic and transport properties of aqueous species at high pressures and temperatures: correlation algorithms for ionic aqueous species and equation of state predictions to 5 kb and 1000 °C, Geochim. Cosmochim. Acta 52 (1988) 2009–2036.
[21] S. Salvi, G.S. Pokrovski, J. Schott, Experimental investigation of aluminum–silica aqueous complexing at 300 °C, Chem. Geol. 151 (1998) 51–67.
[22] S.L. Phillips, F.V. Hale, L.F. Silvester, M.D. Siegel, Thermodynamic tables for nuclear waste isolation, an aqueous solutions database, Report NUREG/CR-4864 LBL-22860 SAND87-0323, Lawrence Berkeley Laboratory, Berkeley California, 1988.
[23] D. Sverjensky, E.L. Shock, H.C. Helgeson, Prediction of the thermodynamic properties of aqueous metal complexes to 1000 °C and 5 kbar, Geochim. Cosmochim. Acta 61 (1997) 1359–1412.
[24] D.D. Wagman, W.H. Evans, V.B. Parker, R.H. Schumm, I. Halow, S.M. Bailey, K.L. Churney, R.L. Nuttall, The NBS tables of chemical thermodynamic properties: selected values for inorganic and C1 and C2 organic substances in SI units, J. Phys. Chem. Ref. Data 11 (Supplement No. 2) (1982).
[25] I. Grenthe, J. Fuger, R.J.M. Konings, R.J. Lemire, A.B. Muller, C. Nguyen-Trung, H. Wanner, Chemical Thermodynamics of Uranium, North-Holland, Amsterdam, 1992.
[26] W. Wagner, A. Pruss, The IAPWS Formulation 1995 for the Thermodynamic Properties of Ordinary Water Substance for General and Scientific Use, J. Phys. Chem. Ref. Data 31 (2002) 387–535.
[27] V.A. Pokrovskii, H.C. Helgeson, Thermodynamic properties of aqueous species and the solubilities of minerals at high pressures and temperatures: the system Al_2O_3–H_2O–NaCl, Am. J. Sci. 295 (1995) 1255–1342.
[28] V.A. Pokrovskii, H.C. Helgeson, Thermodynamic properties of aqueous species and the solubilities of minerals at high pressures and temperatures: the system Al_2O_3 H_2O KOH, Chem. Geol. 137 (1997) 221–242.
[29] E.L. Shock, D.C. Sassani, M. Willis, D.A. Sverjensky, Inorganic species in geologic fluids: correlations among standard molal thermodynamic properties of aqueous ions and hydroxide complexes, Geochim. Cosmochim. Acta 61 (1997) 907–950.
[30] D. Garvin, V.B. Parker, H.J. White, CODATA Series on Thermodynamic Properties, Hemisphere, Washington DC, 1987.
[31] R.P. Bell, J.H.B. George, Trans. Faraday Soc. 49 (1953) 619–627.
[32] V. Pokrovskii, H.C. Helgeson, Calculation of the standard partial molal thermodynamic properties of KCl0 and activity coefficients of aqueous KCl at temperatures and pressures to 1000 °C and 5 kbar, Geochim. Cosmochim. Acta 61 (1997) 2175–2183.
[33] A.E. Martell, R.M. Smith, NIST Critical Stability Constants of Metal Complexes, version 4.0, NIST Database, 46, 1997, Texas A&M University, USA.
[34] C.F. Baes Jr., R.E. Mesmer, The Hydrolysis of Cations, Wiley Interscience, 1976.
[35] D.K. Nordstrom, L.N. Plummer, D. Langmuir, E. Busenberg, H.M. May, B.F. Jones, D.L. Parkhurst, Revised chemical equilibrium data for major water–mineral reactions and their limitations, in: R.L. Bassett, D. Melchior (Eds.), Chemical Modeling in Aqueous Systems II, Symposium Series, 416, 1990, pp. 398–413, American Chemical Society, Colombus.

[36] G.S. Pokrovski, J. Schott, A.S. Sergeyev, Experimental determination of the stability constants of NaSO4- and NaB (OH)40 in hydrothermal solutions using a new high-temperature sodium-selective glass electrode — implications for boron isotopic fractionation, Chem. Geol. 124 (1995) 253–265.

[37] H.C. Helgeson, J.M. Delany, H.W. Nesbitt, D.K. Bird, Summary and critique of the thermodynamic properties of rock-forming minerals, Am. J. Sci. 278A (1978) 1–229.

[38] R.B. Perkins, C.D. Palmer, Solubility of $Ca_6(Al[OH]_6)_2SO_4\cdot 26H_2O$, the chromate analog of ettringite, 5–75 °C, Appl. Geochem. 15 (2000) 1203–1218.

[39] L.S. Wells, W.F. Clarke, H.F. McMurdie, Study of the system $CaO–Al_2O_3–H_2O$ at temperatures of 21° and 90 °C, J. Res. Natl. Bur. Stand. (1943) 367–407.

[40] R.B. Peppler, L.S. Wells, The system of lime, alumina, water from 50° to 250 ° C, J. Res. Natl. Bur. Stand. 52 (1954) 75–92.

[41] F.P. Glasser, M. Tyrer, K. Quillin, D. Ross, J. Pedersen, K. Goldthorpe, D. Bennett, M. Atkins, The chemistry of blended cements and backfills intended for use in radioactive waste disposal, Research and Development Technical Report P98, UK Environment Agency, 1998.

[42] V.I. Babushkin, G.M. Matveyev, O.P. Mchedlov-Petrossyan, Thermodynamics of Silicates, Springer-Verlag, New York, 1985.

[43] C.J.M. Houtepen, H.N. Stein, The enthalpies of formation and of dehydration of some AFm phases with singly charged anions, Cem. Concr. Res. 6 (1976) 651–658.

[44] R.B. Perkins, C.D. Palmer, Solubility of ettringite ($Ca_6[Al(OH)_6]_2(SO_4)_3\times 26H_2O$) at 5–75 °C, Geochim. Cosmochim. Acta 63 (1999) 1969–1980.

[45] M. Atkins, D.G. Bennet, A.C. Dawes, F.P. Glasser, A. Kindness, D. Read, A thermodynamic model for blended cements, Cem. Concr. Res. 22 (1992) 497–502.

[46] D. Damidot, F.P. Glasser, Thermodynamic investigation of the $CaO–Al_2O_3–CaSO_4–H_2O$-system at 50 °C and 85 °C, Cem. Concr. Res. 22 (1992) 1179–1191.

[47] M. Atkins, F.P. Glasser, A. Kindness, Cement hydrate phases: solubility at 25 °C, Cem. Concr. Res. 22 (1992) 241–246.

[48] M. Atkins, F. Glasser, L.P. Moroni, J.J. Jack, Thermodynamic Modeling of Blended Cements at Elevated Temperatures (50 °C–90 °C), DOE Report No. DOE/HMIP/RR/94.011, 1993, D.O.E.

[49] H.A. Berman, E.S. Newman, Heat of formation of calcium aluminate monosulfate at 25 °C, J. Res. Natl. Bur. Stand. A, Phys. Chem. 67A (1963) 1–13.

[50] J. Ederova, V. Satava, Heat capacities of C3AH6, C4ASH12 and C6AS3H32, Thermochim. Acta 31 (1979) 126–128.

[51] M. Schoenitz, A. Navrotsky, Enthalpy of formation of katoite Ca3Al2[(OH)4]3: energetics of the hydrogarnet substitution, Am. Mineral. 84 (1999) 389–391.

[52] D.G. Bennett, D. Read, M. Atkins, F.P. Glasser, A thermodynamic model for blended cements II: cement hydrate phases; thermodynamic values and modelling studies, J. Nucl. Mater. 190 (1992) 315–325.

[53] C.J. Warren, E.J. Reardon, The solubility of ettringite at 25 °C, Cem. Concr. Res. 24 (1994) 1515–1524.

[54] H.F.W. Taylor, Cement Chemistry, 2nd editionThomas Telford, London, 1992.

[55] J. Stark, B. Moser, A. Eckart, New approaches to cement hydration, Part 1, Zem. Kalk Gips 54 (2001) 52–60.

[56] M. Atkins, F. Glasser, L.P. Moroni, J.J. Jack, Thermodynamic Modeling of Blended Cements at Elevated Temperatures (50 °C–90 °C), DOE Report No. DOE/HMIP/RR/94.011, 1993, D.O.E.

[57] E.T. Carlson, The system lime–alumina–water at 1 °C, J. Res. Natl. Bur. Stand. 61 (1958) 1–11.

[58] P.S. de Silva, F.P. Glasser, Phase relations in the system $CaO–Al_2O_3–SiO_2–H_2O$ relevant to metakaolin – calcium hydroxide hydration, Cem. Concr. Res. 23 (1993) 627–639.

[59] D. Damidot, F.P. Glasser, Investigation of the $CaO–Al_2O_3–SiO_2–H_2O$ system at 25 °C by thermodynamic calculations, Cem. Concr. Res. 25 (1995) 22–28.

[60] T.G. Jappy, F.P. Glasser, Synthesis and stability of silica-substituted hydrogarnet $Ca_3Al_2Si_{3-x}O_{12-4x}(OH)_{4x}$, Adv. Cem. Res. 4 (1992) 1–8.

[61] R.A. Robie, B.S. Hemingway, Thermodynamic properties of minerals and related substances at 298.15 K and 1 Bar (105 Pascals) pressure and at higher temperatures, U.S. Geol. Surv. Bull. 2131 (1995) 461 pp.

[62] D. Damidot, S. Stronach, A. Kindness, M. Atkins, F.P. Glasser, Thermodynamic investigation of the $CaO–Al_2O_3–CaCO_3–H_2O$ system at 25 °C and the influence of Na2O, Cem. Concr. Res. 24 (1994) 563–572.

[63] U.A. Birnin-Yauri, F.P. Glasser, Friedel's salt, $Ca_2Al(OH)_6(Cl, OH)\cdot 2H_2O$: its solid solutions and their role in chloride binding, Cem. Concr. Res. 28 (1998) 1713–1724.

[64] J.V. Bothe Jr, P.W. Brown, PhreeqC modeling of Friedel's salt equilibria at 23 °C, Cem. Concr. Res. 34 (2004) 1057–1063.

[65] K.L. Scrivener, A. Fullmann, E. Gallucci, G. Walenta, E. Bermejo, Quantitative study of Portland cement hydration by X-ray diffraction/Rietveld analysis and independent methods, Cem. Concr. Res. 34 (2004) 1541–1547.

[66] B.A. Clark, P.W. Brown, Phases formed from the hydration of tetracalcium aluminoferrite and magnesium sulphate, Adv. Cem. Res. 11 (1999) 133–137.

[67] K.A. Ghanbari, J.H. Sharp, W.E. Lee, Hydration of refractory oxides in castable bond systems — I: alumina, magnesia, and alumina–magnesia mixtures, J. Eur. Ceram. Soc. 22 (2004) 495–503.

[68] M. Altmaier, V. Metz, V. Neck, R. Müller, Th. Fanghänel, Solid–liquid equilibria of $Mg(OH)_2$(cr) and $Mg_2(OH)_3Cl\cdot 4H_2O$(cr) in the system $Mg–Na–H–OH–Cl–H_2O$ at 25 °C, Geochim. Cosmochim. Acta 67 (2003) 3595–3601.

[69] D.K. Nordstrom, L.N. Plummer, D. Langmuir, E. Busenberg, H.M. May, B.F. Jones, D.L. Parkhurst, Revised chemical equilibrium data for major water–mineral reactions and their limitations, in: R.L. Bassett, D. Melchior (Eds.), Chemical Modeling in Aqueous Systems II, Symposium Series, 416, 1990, pp. 398–413, American Chemical Society, Colombus.

[70] P.B. Hostetler, The stability and surface energy of Brucite in water at 25 °C, Am. J. Sci. 261 (1963) 238–258.

[71] E. Königsberger, L.C. Könisberger, H. Gamsjäger, Low-temperature thermodynamic model for the system $Na_2CO_3–MgCO_3–CaCO_3–H_2O$, Geochim. Cosmochim. Acta 63 (1999) 3105–3119.

[72] C.A. Johnson, F.P. Glasser, Hydrotalcite-like minerals ($M_2Al(OH)_6(CO_3)_{0.5}.XH_2O$, where M = Mg, Zn, Co, Ni) in the environment: synthesis, characterization and thermodynamic stability, Clays Clay Miner. 51 (2003) 1–8.

[73] R.K. Allada, E. Peltier, A. Navrotsky, W.H. Casey, C.A. Johnson, H.T. Berbeco, D.L. Sparks, Calorimetric determination of the enthalpies of formation of hydrotalcite-like solids and their use in the geochemical modeling of metals in natural waters, Clays Clay Miner. 54 (2006) 409–417.

[74] J.A. Chermak, J.D. Rimstidt, Estimating the thermodynamic properties (ΔGf^0) of silicate minerals at 298 K from the sum of polyhedral contributions, Am. Mineral. 74 (1989) 1023–1031.

[75] W. Schwarz, Novel cement matrices by accelerated hydration of the ferrite phase in Portland cement via chemical activation: kinetics and cementitious properties, Adv. Cem. Based Mater. 2 (1995) 189–200.

[76] A. Emanuelson, S. Hansen, Distribution of iron among ferrite hydrates, Cem. Concr. Res. 27 (1997) 1167–1177.

[77] J. Csizmadia, G. Balazs, F.D. Tamas, Chloride ion binding capacity of aluminoferrite, Cem. Concr. Res. 31 (2001) 577–588.

[78] G. Möschner, B. Lothenbach, J. Rose, A. Ulrich, R. Figi, R. Kretzschmar, Solubility of Fe-ettringite ($Ca_6[Fe(OH)_6]_2(SO_4)_3\cdot 26H_2O$), Geochim. Cosmochim. Acta 72 (2008) 1–18.

[79] J. Rose, A. Bénard, S. El Mrabet, A. Masion, I. Moulin, V. Briois, L. Olivi, J.-Y. Bottero, Evolution of iron speciation during hydration of C4AF, Waste Manage. 26 (2006) 720–724.

[80] P. Blanc, P. Piantone, A. Lassin, A. Burnol, Thermochimie: Sélection de constantes thermodynamiques pour les éléments majeurs, le plomb et le cadmium, Rapport BRGM 54902-FR, 2006.

[81] M. Grivé, The linkage between uranium, iron and carbon cycle. Process at interfaces: evidences from combined solution chemical and spectroscopic studies, UPC Ph. D. Thesis (2005).

[82] P. Blanc, Thermochimie — Sélection de constantes thermodynamiques pour les zéolites, Rapport BRGM/RP-56854-FR, 2008.

[83] J. Ganguly, S.K. Saxena, Mixtures and Mineral Reactions, Springer-Verlag, 1987.

[84] D. Savage, C. Walker, R.C. Arthur, C.A. Rochelle, C. Oda, H. Takase, Alteration of bentonite by hyperalkaline fluids: a review of the role of secondary minerals, Phys. Chem. Earth 32 (2007) 287–297.

[85] D.E. Rogers, L.P. Aldridge, Hydrates of calcium ferrites and calcium aluminoferrites, Cem. Concr. Res. 7 (1977) 399–409.

[86] R. Rinaldi, M. Sacerdoti, E. Passaglia, Strätlingite: crystal structure, chemistry, and a reexamination of its polytype vertumnite, Eur. J. Mineral. 2 (1990) 841–849.

[87] A.E. Moore, H.F.W. Taylor, Crystal structure of ettringite, Acta Crystallogr. 826 (1970) 386–393.

[88] L. Mercury, P. Vieillard, Y. Tardy, Thermodynamic of ice polymorphs and " Ice-like " water in hydrates and hydroxides, Appl. Geochem. 16 (2001) 161–181.

[89] D.E. Macphee, S.J. Barnett, Solution properties of solids in the ettringite–thaumasite solid solution series, Cem. Concr. Res. 34 (2004) 1591–1598.

[90] T. Schmidt, B. Lothenbach, M. Romer, K. Scrivener, D. Rentsch, R. Figi, A thermodynamic and experimental study of the conditions of thaumasite formation, Cem. Concr. Res. 38 (2008) 337–349.

[91] D. Damidot, S.J. Barnett, D. Macphee, F.P. Glasser, Investigation of the $CaO–Al_2O_3–SiO_2–CaSO_4–CaCO_3–H_2O$ system at 25 °C by thermodynamic calculation, Adv. Cem. Res. 16 (2004) 69–76.

[92] B. Albert, B. Guy, D. Damidot, Water chemical potential: a key parameter to determine the thermodynamic stability of some hydrated cement phases in concrete? Cem. Concr. Res. 36 (2006) 783–790.

[93] S. Antiohos, S. Tsimas, Investigating the role of reactive silica in the hydration mechanisms of high-calcium fly ash/cement systems, Cem. Concr. Compos. 27 (2006) 171–181.

[94] N.C. Collier, N.B. Milestone, J. Hill, I.H. Godfrey, Immobilisation of Fe floc: Part 2, encapsulation of floc in composite cement, J. Nucl. Mater. 393 (2009) 92–101.

[95] P.S. de Silva, F.P. Glasser, Phase relations in the system $CaO–Al_2O_3–SiO_2–H_2O$ relevant to metakaolin – calcium hydroxide hydration, Cem. Concr. Res. 23 (1993) 627–639.

[96] F.P. Glasser, J. Marchand, E. Samson, Durability of concrete — degradation phenomena involving detrimental chemical reactions, Cem. Concr. Res. 38 (2008) 226–246.

[97] H.J. Kuzel, Initial hydration reactions and mechanisms of delayed ettringite formation in Portland cements, Cem. Concr. Compos. 18 (1996) 195–203.

[98] N. Meller, K. Kyritsis, C. Hall, The hydrothermal decomposition of calcium monosulfoaluminate 14-hydrate to katoite hydrogarnet and [beta]-anhydrite: an in-situ synchrotron X-ray diffraction study, J. Solid State Chem. 182 (2009) 2743–2747.

[99] F. Rassineux, J.C. Petit, A. Meunier, Ancient analogues of modern cement: calcium hydrosilicates in mortars and concretes from galloroman thermal baths of Western France, J. Am. Ceram. Soc. 72 (1989) 1026–1032.

[100] D.M. Roy, Alkali-activated cements opportunities and challenges, Cem. Concr. Res. 29 (1999) 249–254.

[101] J.F. MacDowell, Strätlingite and hydrogarnet from calcium aluminosilicate glass cements, Mater. Res. Soc. Symp. Proc. 179 (1991) 159–179.

[102] D. Sawaki, E. Sakai, Characterization for long-aged hardened cement collected from old structures by modern technique for chemical analysis, J. Adv. Concr. Technol. 5 (2009) 325–332.